공학박사 학위논문

Synthesis and Characterization of Amphiphilic Polymeric Materials Having Interfacial Activity for Water Treatment Membrane and Polymer Nanocomposite Applications

계면 활성을 지닌 양친매성 고분자 재료의 합성과 분석, 그리고 수처리 막 및 고분자 나노복합체로의 응용

2020년 8월

서울대학교 대학원

화학생물공학부

정 경 화

Synthesis and Characterization of Amphiphilic Polymeric Materials Having Interfacial Activity for Water Treatment Membrane and Polymer Nanocomposite Applications

by

Kyung Hwa Jung

Adviser: Professor Jong-Chan Lee, Ph. D.

Submitted in Partial Fulfillment
of the Requirements for the Degree of
DOCTOR OF PHILOSOPHY

August 2020

School of Chemical and Biological Engineering
College of Engineering
Graduate School
Seoul National University

Abstract

Synthesis and Characterization of Amphiphilic Polymeric Materials Having Interfacial Activity for Water Treatment Membrane and Polymer Nanocomposite Applications

정 경 화 (Kyung Hwa, Jung)

공과대학 화학생물공학과 (Chemical and Biological Engineering)

고분자 합성 전공 (Polymer Synthesis)

The Graduate School

Seoul National University

This study presents the synthesis and characterization of amphiphilic polymeric materials having interfacial activity for water treatment (such as ultrafiltration and reverse osmosis membranes) and polymer nanocomposite applications. Firstly, ultrafiltration membranes coated with amphiphilic copolymers containing superhydrophilic zwitterionic moieties and hydrophobic POSS moieties (PSM-coated membranes) were prepared. The free-radical polymerization of 2-(dimethylamino)ethyl methacrylate (DMAEMA) and 3-(3, 5, 7, 9, 11, 13, 15-

heptaisobutylpentacyclo[9.5.1.1^{3,9}.1^{5,15}.1^{7,13}]octasiloxane-1-yl)propyl methacrylate (MAPOSS) monomers was used to prepare a series of copolymers containing different compositions of DMAEMA and MAPOSS units (PDMs). The DMAEMA units in the PDM-coated membranes were subsequently converted to sulfobetaine methacrylate (SBMA) units using 1,3-propane sultone (post-zwitterionization) to give the PSM-coated membranes. The PSM-coated membranes showed the best fouling resistance/release properties. The improved fouling resistance properties of the PSM-coated membranes were attributed to the superhydrophilic zwitterionic moieties, which form a hydration layer on the membrane surface v*ia* electrostatic interactions between the zwitterions and water molecules. Moreover, the total surface energy (γ_S) value of the PSM-coated membrane is smaller than that of the PSf membrane due to the hydrophobic POSS moieties. This results in the superior fouling release properties of the PSM-coated membranes.

Secondly, a well-defined water-soluble superamphiphilic block copolymer surfactant containing superhydrophilic zwitterionic and very hydrophobic long alkyl units (PS*b*PDz) was synthesized *via* reversible addition-fragmentation chain-transfer polymerization for

the replacement of the conventional surfactant used to polyamide (PA) thin-film reverse osmosis (RO) membrane. PS*b*PDz was found to act as a surfactant successfully, and work as a filler at the same time even after interfacial polymerization (IP) due to its entanglement effect of the polymer chains with the PA matrix. As the surfactant, PS*b*PDz improves the water wettability on the top surface of the support layers and expands the interface area between the aqueous and organic phase, decreasing the thickness and increasing the roughness of the PA selective layer, respectively. As the filler, PS*b*PDz introduced into the PA selective layer increases the water wettability of the RO membrane. Hence, the RO membrane fabricated with PS*b*PDz in the aqueous solution through IP shows the largest water flux value than the neat RO membrane maintaining the high salt rejection value.

Finally, poly(phenylene sulfide)/nylon 6 grafted graphene oxide (PPS/NGO) nanocomposites were prepared by micro-compounding, where NGO was prepared *via* ring-opening polymerization of ε-caprolactam on the surface of the graphene oxide (GO), which has carboxylic acid groups that can act as an initiation group. Since nylon 6 is known to be blended with PPS in commercial, the nylon 6 moieties in NGO can increase the mechanical properties of PPS,

especially resulting in PPS/NGO nanocomposites with improved toughness. Moreover, graphene nanosheets can provide improved mechanical strength and thermal stability because of their mechanical reinforcing and thermal barrier effects. As a result, PPS/NGO nanocomposite showed the best mechanical properties (such as the tensile strength and elongation at break values) and the enhanced thermal stability. These improved properties can be ascribed to the well-dispersed NGO in the PPS matrix, as confirmed by the morphology studies using SEM and EDS mapping analysis.

Keywords: Surface coating, amphiphilic zwitterionic random copolymers, water treatment, membranes, antifouling properties, thin-film composite, amphiphilic zwitterionic block copolymer, surfactant, filler, desalination, poly(phenylene sulfide), graphene oxide, engineering plastics, nanocomposite

Student Number: 2014-22620

TABLE OF CONTENTS

Chapter 3

Superamphiphilic Zwitterionic Block Copolymer Surfactant-assisted Fabrication of Polyamide Thin-film Composite Membrane with Ultra-high Flux for Water Desalination

Chapter 4

Preparation of Poly(phenylene sulfide) / Nylon 6 Grafted Graphene Oxide Nanocomposites with Enhanced Mechanical and Thermal Properties

List of Tables

Table 4.2. Thermal and mechanical properties of neat PPS and PPS/NGO nanocomposites.

List of Figures

with PS*b*PDz, and SDS. (c) Contact angle after 140 s for the neat RO membrane, the RO membranes with PS*b*PDz (0.015 wt%), and SDS (0.1 wt%).

Figure 3.3. (a) Schematic diagram for the increase of the wettability of the top surface of the support membrane by the addition of PS*b*PDz. (b) Water contact angles of DI water, PS*b*PDz (0.005 – 0.030 wt%), and SDS (0.1 wt%) aqueous solutions on the support membranes. (c) Schematic diagram for the increase of the interfacial region between aqueous and organic solutions by the addition of PS*b*PDz. (d) Optical microscope image of the hexane droplets in water (0.9 g of hexane in1 L of water) containing 0.015 wt% of PS*b*PDz as the emulsifier.

Figure 3.4. Cross-sectional SEM images of (a) the neat RO membrane, the RO membranes with (b) 0.015 wt% of PS*b*PDz, and (c) 0.1 wt% of SDS.

Figure 3.5. Optical microscope images of the hexane droplets in water (0.9 g of hexane in 1 L of water) containing (a) 0.015 wt% and (b) 0.1 wt% of SDS.

Figure 3.6. SEM images of (a) the neat RO membrane, the RO membranes with (b) 0.015 wt% of PS*b*PDz, and (c) 0.1 wt% of SDS. AFM 3D images of (d) the RO membrane, the RO membranes with (e) 0.015 wt% of PS*b*PDz, and (f) 0.1 wt% of SDS.

Chapter 1

Introduction

Since the advent of polymer science as disciplines, many researchers have attention enormously to develop *amphiphilic* (amphi: of both kinds; philic: having an affinity for) polymeric materials that can be located at various types of interfaces (*e.g.* solid-solid, solid-liquid, and liquid-liquid interfaces) to impart interfacial activity. The "amphiphilicity" in polymer science has the meaning of not only good solubilities in a variety of solvents but also good interfacial activity between different phases.[1] The interfacial active amphiphilic polymeric materials are classified as a new class of functional materials, providing a large number of applications requiring structural control at the material interface, such as coating materials, additives for interfacial polymerization, and compatibilizer for polymer blend and/or nanocomposite applications. One of the most important goals in amphiphilic polymeric materials synthesis has always been that the chemical structure of the amphiphilic polymeric materials should be designed and synthesized to meet the required properties of interfaces with very different chemical properties, polarity, and viscosity.

1.1. Amphiphilic copolymers

The development of synthesis strategies to prepare amphiphilic copolymers with suitable interfacial activity for each application has been significantly progressed in the past few decades. This is owing to the wide variety of the structures of the copolymers that can be achieved by the choice of repeating units, the length of both parts (such as hydrophilic and hydrophobic units), and possible copolymerization techniques.[1] Among the copolymerization techniques, free radical polymerization technique has attracted great attention to synthesizing amphiphilic random copolymers due to their advantages in a practical point of view, such as easy/simple reaction process and good solubility of the resulting polymers in organic solvents.[2, 3] However, such amphiphilic random copolymers often have a limitation in uses for the specific applications requiring super amphiphilic characters, such as interfacial polymerization and polymer blends applications.[4] In that regard, a living radical polymerization technique has been adopted to prepare amphiphilic block copolymers with much more amphiphilicity than amphiphilic random copolymers with the same repeating units and degree of polymerization.[5] Nonetheless, such technique in practical uses is still hampered by problems such as many steps,

difficult/complex reactions, and cost issues. Hence, polymer scientists are required to synthesis amphiphilic random or block copolymers using proper copolymerization techniques based on the properties required in each application.

1.2. Polymer grafted nanomaterials

Since the development of various nanomaterials such as carbon- and metal-based nanomaterials, it is now clearly accepted that the addition of nanomaterials into polymer resins has an advantage in their mechanical, chemical, electrical, and/or optical properties.[6] It is also well-known that the uniform dispersion state of nanomaterials in a polymer matrix is required to optimize the desired properties of polymer nanocomposites.[7] However, it still remains as challenges to obtain the polymer nanocomposites in which such nanomaterials are evenly dispersed in the polymer matrix because of their strong aggregation characteristics.[8] Multiple strategies to control the nanomaterials dispersion in the polymer matrix have been suggested such as size control of nanomaterials, surface oxidation, and polymer grafting techniques. Among them, polymer grafting technique onto the

surface of nanomaterials has attracted considerable attention because polymer brushes grafted on the surface of nanomaterials can improve the miscibility of nanomaterials within the polymer matrix, resulting in control of dispersion.[9] Considerable work on polymer nanocomposites application shows that the dispersion of nanomaterials in the polymer matrix can be controlled by various factors such as the type of repeating units of the grafted polymer, the grafting density, and chain length.[10] Hence, it is still challenging to optimize the dispersion state of polymer grafted nanomaterials, resulting in the preparation of outstanding polymer nanocomposite in polymer science.

1.3. Motivation

Based on the understanding of unique features of amphiphilic polymeric materials including amphiphilic (random and/or block) copolymers and polymer grafted nanomaterials, various amphiphilic polymeric materials having interfacial activity are designed and prepared for various applications such as water treatment membranes and polymer nanocomposites. The main drawback of conventional water treatment membranes is a lack of long-term stability due to the

fouling phenomenon, especially in ultrafiltration membranes where various organic molecules (such as proteins, humic acids, and oils) are filtered fastly and adsorbed subsequently on the membrane. Additionally, although lots of efforts have been performed to break the trade-off behavior between flux and salt rejection in water treatment membranes, nanofiltration and/or reverse osmosis membranes fabricated using interfacial polymerization process is still suffering from the trade-off phenomenon. Such limitations in water treatment membranes can be overcome by the coating of amphiphilic random copolymer onto the surface of the ultrafiltration membrane, and by the addition of amphiphilic block copolymer to the aqueous solution for control of interfacial polymerization parameters, respectively. The main issue to improve the properties of polymer nanocomposites using engineering plastics as the polymer matrix is hard to obtain uniform dispersion state of nanomaterials in the engineering plastics matrix due to very low miscibility. This disadvantage can be controlled by grafting polymers, which has strong interaction with polymer chains of engineering plastics, onto the surface of nanomaterials.

1.4. References

[1] S. Forster, M. Antonietti, *Adv. Mater.,* **1998**, 10, 195.

[2] I. Sadeghi, A. Asatekin, *Macromol. Chem. Phys.,* **2017**, 20, 1700226.

[3] H. Lambermont-Thijs, R. Hoogenboom, C.-A. Fustin, C. Bomal-D'Haese, J.-F. Gohy, U. S. Schubert, *J. Polym. Chem. Part A,* **2008**, 2, 515.

[4] Y. Lyatskaya, D. Gersappe, N. A. Gross, A. C. Balazs, *J. Phys. Chem.,* **1996**, 100, 1449.

[5] K. Matyjaszewski, *Curr. Opin. Solid State Interface Sci.* **1996**, 1, 769

[6] M. R. Bockstaller, R. A. Mickiewicz, E. L. Thomas, *Adv. Mater.,* **2005**, 17, 1331.

[7] S. K. Kumar, N. Jouault, *Macromolecules,* **2013**, 46, 3199.

[8] M. Y. Lim, H. J. Kim, S. J. Baek, K. Y. Kim, S. S. Lee, J. -C. Lee, *Carbon*, **2014**, 77, 366.

[9] R. Hasegawa, Y. Aoki, M. Doi, *Macromolecules*, **1996**, 29, 6656−6662.

[10] C. R. Iacovella, M. A. Horsch, S. C. Glotzer, *J. Chem. Phys.*, **2008**, 129, 044902.

Chapter 2

Ultrafiltration Membranes Coated by Amphiphilic Copolymers Containing Superhydrophilic Zwitterionic and Hydrophobic POSS Moieties Showing Improved Fouling Resistance/Release Properties

2.1. Introduction

In an effort to resolve the current global water shortage problems, there have been significant efforts to develop water purification technologies including membrane filtration (*e.g.*, microfiltration (MF), ultrafiltration (UF), nanofiltration (NF), and reverse osmosis (RO)), thermal/membrane distillations, and electrodialysis. Among them, the membrane filtration technology has been studied and applied widely because of the advantages such as high selectivity, low cost, low energy consumption, and fast production rate.[1-3] However, membrane fouling caused by the attachment of the foulants on the membrane surface during the filtration process is the main obstacle to increase membrane operation times and to reduce the operation costs.[4-9] Therefore, the development of water filtration membranes that can maintain high water flux without much foulant attachment keeps progressing.[10-13]

Various strategies have been developed to prevent membrane fouling by a variety of foulants. Especially, membrane surface modification by hydrophilic moieties such as poly(ethylene glycol) (PEG),[11, 14-16] zwitterions,[10] and bio-based polymers[17-19] has been widely

studied to prepare the membranes having antifouling properties. Still, these membranes surface-modified with hydrophilic materials have suffered from the fouling issues by hydrophobic foulants. For example, oils could be adsorbed and easily deformed to a continuous layer, subsequently covering a large area of the membrane surface resulting in a significant decrease of water flux.[20] Therefore, in addition to the fouling resistance ability, the fouling release ability has been considered to be very important to improve membrane performance.[21] Functional groups having low surface energy (*e.g.*, silicone- or fluorine-moieties) have been used to impart fouling release properties by weakening the interfacial interaction of the foulants with the membrane surface.[22, 23] As a more advanced technology, the introduction of amphiphilic surfaces having both hydrophilic and hydrophobic moieties have also been reported to be effective as dual activity materials with the fouling resistance and fouling release.[11, 12, 14, 17, 24] Since zwitterions can impart superhydrophilicity, amphiphilic copolymers having zwitterionic moieties have been also developed. However, since many of the polymers having zwitterionic moieties have poor solubility in most of the organic solvents,[10, 25, 26] their application in the surface coating process, the most efficient way

to modify the membrane surface,[12] has been limited.

Herein, we report our strategy to prepare the UF membranes having both superhydrophilic zwitterionic and hydrophobic POSS moieties. This amphiphilic membrane surface could be prepared by a surface coating of a precursor polymer followed by the post surface modification process. Since hydration layers can be formed on the membrane surface by the strong electrostatic interaction between zwitterions and water molecules, they could act as a barrier layer for the foulants, decreasing the fouling rate.[27-30] Besides, the POSS functional group, having multi-silicon moiety, can lower the total surface energy (γ_S) of the membrane surface, thus improving the fouling release property.[31-34] This research could provide a practical strategy to prepare the filtration membranes with a long lifetime.

2.2. Experimental

2.2.1. Materials

2,2′-Azobisisobutyronitrile (AIBN, Junsei) was recrystallized from

ethanol (EtOH, Daejung Chemicals) below 0 ºC prior to use. 2-(Dimethylamino)ethyl methacrylate (DMAEMA, 98 %, Sigma–Aldrich) was purified by passing through a syringe filter (0.2 μm, Whatman) filled with aluminum oxide (basic, for chromatography, 50 – 200 μm, Acros Organics) immediately before polymerization. 3-(3, 5, 7, 9, 11, 13, 15-heptaisobutylpentacyclo[9.5.1.1^{3,9}.1^{5,15}.1^{7,13}]octasiloxane-1-yl)propyl methacrylate (MAPOSS) was purchased from Hybrid Plastics (product no. MA0702) and used as received. Tetrahydrofuran (THF, > 99 %, Daejung Chemicals) was distilled over sodium/benzophenone under a nitrogen atmosphere. Polysulfone (PSf, PS20 from SePRO Corporation) ultrafiltration membrane was stored in distilled water. Isopropanol (IPA, Daejung Chemicals), bovine serum albumin (BSA, M_w = 67 kDa, Millipore–Sigma), sodium dodecyl sulfate (SDS, > 99 %, Fluka) and vacuum pump oil (Mobil) were obtained from commercial sources and used as received. All other chemicals were used as received from Millipore–Sigma unless otherwise specified.

2.2.2. Synthesis of poly(2-dimethylamino)ethyl methacrylate-*r*-methacryloisobutyl POSS) (PDM)

The abbreviation of poly(2-(dimethylamino)ethyl methacrylate-*r*-methacryloisobutyl POSS) is PDM#, where # is the molar content of the MAPOSS unit in the polymer. The general procedure for the synthesis of the PDMs is detailed using PDM15 (containing 85 mol% of DMAEMA units and 15 mol% of MAPOSS monomeric units) as a representative example: DMAEMA (1.069 g, 6.8 mmol), MAPOSS (1.156 g, 1.2 mmol), and AIBN (6.568 mg, 0.04 mmol) were dissolved in distilled THF (15 mL) and subsequently placed into a 50 mL Schlenk flask equipped with a magnetic stirring bar and a condenser. The mixture was deoxygenated by a freeze-pump-thaw cycle, and the reaction was performed in an oil bath thermostatted at 80 ^{o}C for 24 h under nitrogen atmosphere. The resultant product was purified by precipitation in deionized (DI) water several times. The resulting white solid was filtered and dried under vacuum at room temperature for several days. A schematic illustration of the synthesis of the PDM is presented in **Figure 2.1a.**

2.2.3. Preparation of PDM- and PSM-coated membranes

The PSf ultrafiltration membrane was immersed in an IPA-bath for

10 min to activate the pores and was then washed several times with DI water. The IPA-treated PSf membrane was placed in a water bath for 3 h to stabilize the pores. A PDM solution (0.05 wt% in hexane, 1 mL) was spin-coated onto the PSf membrane (5000 rpm, 160 s), and the membrane was then dried in a vacuum oven at 35 ºC for 24 h. The PDM-coated membrane was immersed in a vial containing an aqueous solution of 1, 3–propane sultone (0.1 wt%) for 24 h for the post-zwitterionization of the DMAEMA units to produce the PSM-coated membrane. The resulting membrane was washed with DI water for 10 min.

2.2.4. Membrane filtration tests

Membrane filtration tests were conducted using dead-end filtration cells (CF042, Sterlitech Corp., Kent, WA) with an effective filtration area of $1.3 \times 1.3 \times \pi$ cm^2. The pressure was maintained at about 1 bar by N_2 gas, and all the filtration tests were conducted at ambient temperature. The pure water flux value, J_{w1} (L m^{-2} h^{-1}, LMH), was calculated from the volume of the permeated water after 1 h of filtration. A BSA solution (1 g L^{-1}) or an oil/water emulsion (0.9 g L^{-1}

of oil and 0.1 g L^{-1} of SDS) was used as a feed solution to evaluate the fouling resistance properties. The membrane surface was washed with DI water after set times during the filtration experiments (2 and 4 h), and then the water flux of the as-cleaned membranes was measured in order to analyze the fouling release properties of the membranes. Flux-recovery was evaluated using several parameters, including flux recovery ratio (FRR), the total flux-decline ratio (DR_t), the reversible flux-decline ratio (DR_r), and the irreversible flux-decline ratio (DR_{ir}).

$$FRR = J_{w2}\,(\text{or } J_{w3}) / J_{w1} \times 100\ \% \quad (1)$$

$$DR_t = [1 - J_p / J_{w1}] \times 100\ \% \quad (2)$$

$$DR_r = [J_{w2}\,(\text{or } J_{w3}) - J_p] \times 100\% \quad (3)$$

$$DR_{ir} = [J_{w1} - J_{w2}\,(\text{or } J_{w3})] / J_{w1} \times 100\% \quad (4)$$

where J_{w1} is the initial flux and J_p is the flux recorded at each time. Water flux values of the cleaned membranes at 2 and 4 h after initial feeding were recorded as J_{w2} and J_{w3}, respectively. All filtration experiments for the samples were repeated more than three times to confirm reproducibility.

2.2.5. Characterization

^{1}H nuclear magnetic resonance (^{1}H NMR) spectra were obtained using a Bruker Avance III 400 FT–NMR. Number-average and weight-average molecular weights (M_n and M_w) and the dispersity (Đ) were obtained by size exclusion chromatography (SEC). SEC was performed in THF (30 ºC, 1 mL min^{-1}) on a Waters 515 HPLC system equipped with three Polymer Laboratories columns (a PL gel 5.0 μm guard, MIXED–C, and MIXED–D in series with a Viscotek T60A refractive index detector). The resultant SEC data was analyzed using Omnisec software. The surface compositions of the membranes were evaluated by X-ray photoelectron spectroscopy (XPS, Kratos Inc., AXIS–HSi) using Mg/Al (1486.69 eV) as the radiation source. Survey spectra were collected over a range of 0 – 1500 eV, followed by a high-resolution scan in the C 1s, O 1s, N 1s, and S 2p regions. Surface morphologies and energy dispersive spectroscopy (EDS) were examined by field emission scanning electron microscopY (FESEM, Carl Zeiss, SUPRA 55VP). Contact angles were determined by the sessile drop technique using water as the liquid droplet and were measured by a Krüss DSA10

contact angle analyzer. The contact angles were measured at least five times. Atomic force microscopy (AFM, Park Systems, NX–10) was used to investigate the surface topography of the membranes. An area of 5 μm × 5 μm of the membrane was scanned using non-contact mode at a scan rate of 0.3 Hz under ambient conditions of temperature and humidity.

2.3. Results and Discussion

2.3.1. Synthesis of poly(DMAEMA-*r*-MAPOSS) copolymers (PDMs)

A series of PDMs with different MAPOSS contents were synthesized *via* free radical polymerization (**Figure 2.1a and Table 2.1**). PDMs with a MAPOSS content greater than 10 mol% were targeted for this work because PDMs containing a MAPOSS content lower than 10 mol% are soluble in water, and hence, cannot be used in the water filtration process. The ^{1}H NMR spectrum of a representative copolymer (PDM10) is shown in **Figure 2.2**. The molar ratios of the DMAEMA to the

MAPOSS units in the copolymers were calculated using **Equation 2.5**:

$$\text{MAPOSS content} = (I_{g+j} / 16) [(I_e / 6) + (I_{g+j} / 16)] \times 100 \text{ mol\%} \quad (5)$$

where I_e is the integral value of signal e at 2.3 ppm in the ^{1}H NMR spectrum (corresponding to the methyl protons of dimethylamine in the DMAEMA units), and I_{g+j} is the combined integral values of signals g and j at 0.6 ppm (corresponding to the methylene protons in the MAPOSS units). Although the DMAEMA and MAPOSS monomers likely exhibit different reactivities during polymerization, the molar ratios of DMAEMA and MAPOSS units in the copolymers were found to be similar to the molar ratios of the monomers used in the feedstock (**Table 2.1**).

2.3.2. Post-zwitterionizations of the PDM-coated membranes

The post-zwitterionizations were conducted using PDM-coated membranes. When PDM itself was treated with 1,3-propane sultone to attempt the preparation of the zwitterionic polymers, it was found to be insoluble in most organic solvents, and could not be coated onto the

PSf membrane. The products of the post-zwitterionizations were characterized using XPS and FT-IR (**Figure 2.3**). As shown in **Figure 2.3a**, the characteristic peak corresponding to the C–N bonds in the DMAEMA moieties (397 eV) in the XPS spectrum is shifted to 400 eV, indicating successful zwitterionization to form $C–N^+$ bonds.[13] The intensities of the peaks corresponding to the N 1s and S 2p orbitals (N/S ≈ 1) both increase, which further supports the conclusion of successful zwitterionization (**Table 2.2**). Additionally, to investigate the conversion of DMAEMA units to SBMA units by the post-zwitterionization process at the different coating layer depths, XPS analysis was also performed for the PDM10- and PSM10-coated Si wafers at different angles (0° and 30°), respectively (**Figure 2.4**). The spectra shifting behavior of the spectra at different angles is quite similar, indicating that DMAEMA units in the PDM10 coating layer are converted thoroughly to SBMA units through the post-zwitterionization process at the different coating depths. The post-zwitterionization on the membrane surface was also confirmed by FT-IR analysis (**Figure 2.3b**). The new characteristic peaks appearing at 1150 cm^{-1} and 1040 cm^{-1} correspond to the symmetric and asymmetric stretching of the $–SO_3$ groups, and the peak at 1582 cm^{-1} ($C–N^+$ stretching) provides

evidence of the formation of the quaternary ammonium group. The peaks corresponding to the C=O (1730 cm^{-1}), Si–O–Si (1128 and 1094 cm^{-1}), and $–N(CH_3)_2$ (2823 and 2775 cm^{-1}) groups all decrease in intensity, which provides further indication of the successful post-zwitterionization.[35, 36]

2.3.3. Membrane performances

Figure 2.5 shows the pure water flux (PWF) values of the neat PSf, PDM-, and PSM-coated membranes. The PWF values of the PDM-coated membranes are smaller than the PWF value of the neat PSf membrane because the pores of the PDM-coated membranes are substantially blocked during the PDM coating process, as shown in the surface SEM images (**Figure 2.6).** This has been observed in other studies that have applied polymer coating to the membranes.[11, 15, 17, 18] Additionally, the PWF values of the PDM-coated membranes decrease with increasing MAPOSS content because the MAPOSS units increase the hydrophobicity of the polymer coating.[37-39] After post-zwitterionization, the PWF values increase because the zwitterionic moieties on the membrane surface increase the hydrophilicity of the

polymer coating.[40] These polarity changes on the membrane surface were evaluated by measuring the water contact angles of the membranes using the sessile drop method (**Figure 2.7**).[41] The contact angle of the PSf membrane increases from 75 º (with no PDM coating) to 100 º (when PDM was coated onto the membrane surface). The post-zwitterionization of the PDM-coated membrane to the PSM-coated membrane resulted in a decrease in the contact angle value (corresponding to an increase in the hydrophilicity of the surface). This decrease was less pronounced when the coated polymer contained a larger proportion (> 25 mol%) of MAPOSS units. This is in agreement with results from our previous study on amphiphilic copolymers containing high proportions of hydrophobic moieties.[26]

2.3.4. Fouling resistance/release properties

The fouling resistance properties were studied using a (bovine serum albumin) BSA solution filtration test as a representative protein foulant and an oil/water emulsion as a representative hydrocarbon foulant (**Figure 2.8**). The neat PSf membrane and the PDM-coated membranes experienced a significant decline in their water flux values in the

presence of the BSA foulant. As shown in **Figure 2.8**, the normalized flux values of these membranes decrease by over 40% because the BSA can be readily adsorbed onto the pore surface of these hydrophobic membranes.[42] In particular, the PDM25-coated membrane (which contains the highest proportion of hydrophobic MAPOSS units) is the most significantly affected membrane, showing the greatest decline in its water flux value, and the smallest normalized water flux value overall. Conversely, the PSM-coated membranes show smaller decreases in their water flux values and larger normalized water flux values than the PDM-coated membranes during the BSA solution filtration test. The final normalized flux values for the PSM-coated membranes were found to increase with the increasing zwitterionic character of the polymer coating (**Figure 2.8a**). The improved fouling resistance properties of the PSM-coated membranes against BSA can be attributed to the superhydrophilic zwitterion moieties that can induce the formation of hydration layers on the membrane surface *via* strong electrostatic interactions with water molecules.[28-30] The hydration layer on the membrane surfaces can reduce the number of direct interactions between BSA molecules and the membrane surface, resulting in an increase in fouling resistance. The oil/water emulsion

filtration test was also performed to investigate the fouling resistance properties of the membranes against oils (**Figure 2.8b**). The neat PSf membrane and the PDM-coated membranes experienced a greater decrease in their water flux values (and smaller normalized water flux values overall) when the oil/water emulsion was used as the foulant compared with when BSA was used. This effect was particularly apparent when filtration times were longer (> 40min). The PDM25-coated membrane (the most hydrophobic membranes) once again showed the greatest decline in water flux value, and the smallest normalized water flux value overall (approaching zero). The greater degree of fouling experienced by the membranes in the presence of the oil/water emulsion can be attributed to the characteristic properties of oils; they can be readily deformed and spread over a large surface area on the membrane.[43] Conversely, the PSM-coated membranes show lower decreases in their water flux values, and larger normalized water flux values overall because hydration layers can be efficiently formed on the hydrophilic PSM-coated membrane surface.

To evaluate the fouling release properties of the membranes, the PSM10-coated membrane was selected as the representative membrane because it showed the highest fouling resistance. The neat PSf

membrane and the PDM10-coated membrane were used as the control membranes. Filtration was conducted in the presence of BSA and oil/water emulsion foulants for 350 min, with the membranes being rinsed thoroughly with deionized (DI) water after 120 min and 240 min. The flux parameters such as FRR, DR_t, DR_r, and DR_{ir} were compared (**Figure 2.9 and 2.10**). The fouling release properties can be characterized by comparing the DR_{ir} values of the different membranes. Given that the fouling release materials can decrease the number of irreversible foulants, smaller DR_{ir} values indicate better fouling release properties. The DR_{ir} values of the neat PSf membrane in the BSA solution filtration test are 49 and 53 % at 120 min, and 240 min, respectively; the DR_{ir} values of the PSM10-coated membrane are 13 and 17 % at 120 min, and 240 min, respectively. This indicates that the PSM10-coated membrane has better fouling release properties against BSA than the neat PSf membrane. Fouling release is more important for oil/water emulsion foulants than the BSA foulants. This is because the oil/water foulants can be more readily block the surface area of the membrane than the BSA.[12] The DR_{ir} values of the neat PSf membrane in the oil/water emulsion filtration test are approximately 81 and 88 % at 120 min, and 240 min, respectively; the DR_{ir} values of the

PSM10-coated membrane are significantly smaller (approximately 26 and 34 % at 120 min, and 240 min, respectively). This indicates that the PSM10-coated membrane has far superior fouling release properties than the neat PSf membrane against oil.

One possible hypothesis for the improvements in the fouling resistance/release properties of the PSM-coated membrane is the synergistic effect of the hydration layer (formed due to the zwitterionic moieties) and low surface energy (as a result of the POSS moieties). The surface energies of the representative three membranes, the neat PSF, PDM10-coated, and PSM10-coated membranes, are shown in **Table 2.3.**[24, 44, 45] The total surface free energy (γ_S) was calculated using Owens and Wendt's geometric method, which considers both dispersive (γ_S^D) and polar (γ_S^P) components.

$$\gamma_S = \gamma_S^D + \gamma_S^P \tag{2}$$

$$\gamma_S(1 + \cos\theta) = 2\sqrt{\gamma_S^D \gamma_L^D} + 2\sqrt{\gamma_S^P \gamma_L^P} \tag{3}$$

where θ is the measured contact angle value of liquids on the surface, and γ_L^D and γ_L^P are the dispersive, and polar components, respectively. The PSM10-coated membrane (which shows the best

fouling resistance properties), has the largest γ_S^P value, indicating that it forms the strongest electrostatic interactions between water molecules and the membrane surface. This is likely because it contains highly polar zwitterionic moieties. Although the PSM10-coated membrane is more hydrophilic than the neat PSf membrane (the water contact angle value of the PSM10-coated membrane is smaller than that of the neat PSf membrane), the γ_S value of the PSM10-coated membrane is smaller than that of the neat PSf membrane; this is because PSM10 contains hydrophobic MAPOSS units that have lower surface energy than the PSf monomeric units.[14, 31] This improved hydrophobicity of the PSM10-coated membrane was found to improve the fouling release properties compared with the neat PSf membrane. The most hydrophobic membrane (PDM10-coated membrane), which was found to have the smallest γ_S^P and γ_S values among the three membranes, has the poorest fouling resistance, as shown in **Figure 2.9**. However, this membrane still has better fouling release properties than the neat PSf membrane because it has a smaller γ_S value than the neat PSf membrane, as reported previously.[45, 46] Therefore, the PSM10-coated membrane, which has both superhydrophilic zwitterionic moieties and hydrophobic POSS moieties, shows the best antifouling

properties.

The surface roughness is known to be one of the important factors in determining the antifouling properties of membranes.[47, 48] Smoother surfaces often lead to better antifouling properties.[47-49] Since membranes with rough surfaces have correspondingly larger surface areas, the incidence of fouling can increase as a result of more interactions between the membrane surface and the foulants.[47, 50] The PSM10-coated membrane was found to have a smoother surface than the neat PSf membrane, as observed by atomic force microscopy (AFM), as shown in **Figure 2.11**. The polymer coating can result in a smoothening of the membrane surface, which has been reported previously.[51, 52] Although the small differences in surface roughness between the neat PSf and PSM10-coated membranes may not be the crucial factor in determining membrane performance, it can still have some degree of impact on the antifouling properties.

To study the stability of the polymer coatings, the stability tests were conducted. At first, PDM10- and PSM10-coated membranes were immersed in DI water for 24 h before drying. The compositions of the membranes were analyzed by XPS prior to, and after completion of, the stability test. No changes in the chemical compositions of either

membrane were found upon completion of the 24 h period (**Table 2.4**). Also, the fouling tests for the PSM10-coated membrane were conducted after the filtration of DI water for 3 days, as shown in **Figure 2.11**. The flux value under DI water filtration test does not change much, if any, for 3 days, and the flux decreases under filtration of BSA solution and oil/water emulsion for the long-term were found to be similar to the results obtained from the short-term test in **Figure 2.9**, indicating that the PSM10-coated membrane is stable over the long-term period.

2.4. Conclusions

In this study, we demonstrate that membranes coated with amphiphilic copolymers containing superhydrophilic zwitterionic and hydrophobic POSS moieties (PSM-coated membranes) have promising fouling resistance/release properties against both BSA and oil foulants. The superhydrophilic zwitterionic moieties in the PSM-coated membranes were found to improve the fouling resistance properties by forming hydration layers on the membrane surfaces *via* electrostatic interactions between zwitterions and water molecules. The fouling

resistance properties of these PSM-coated membranes are superior compared with the membranes that do not contain the superhydrophilic zwitterionic moieties, such as the neat PSf membrane, and the PDM-coated membrane. Moreover, the hydrophobic (low surface energy) POSS moieties in the PDM- and PSM-coated membranes were found to improve the fouling release properties compared with the neat PSf membrane. This is due to a reduction in the total surface energies of the PDM- and PSM-coated membranes, compared with the neat PSf membrane. However, given that the PDM-coated membrane has the poorest fouling resistance, the PSM-coated membrane containing both superhydrophilic zwitterionic moieties and hydrophobic POSS moieties was found to have the best antifouling properties. We believe that our results provide insight into the relationship between the compositions of polymers, membrane surface properties, and fouling resistance/release properties.

2.5. References

[1] M. Hightower, S. A. Pierce, *Nature,* **2008,** 452, 285.

[2] M. A. Shannon, P. W. Bohn, M. Elimelech, J. G. Georgiadis, B. J.

Marinas, A. M. Mayes, *Nature,* **2008,** 452, 301.

[3] M. F. A. Goosen, S. S. Sablani, H. Al-Hinai, S. Al-Obeidani, R. Al-Belushi, D. Jackson, *Sep. Sci. Technol.,* **2005,** 39, 2261.

[4] A. L. Lim, R. Bai, *J. Membr. Sci.,* **2003,** 216, 279.

[5] N. Hilal, O. O. Ogunbiyi, N. J. Miles, R. Nigmatullin, *Sep. Sci. Technol.,* **2005,** 40, 1957.

[6] J. Mansouri, S. Harrisson, V. Chen, *J. Mater. Chem.,* **2010,** 20, 4567.

[7] I. Banerjee, R. C. Pangule, R. S. Kane, *Adv. Mater.,* **2011,** 23, 690.

[8] W. Guo, H. H. Ngo, J. Li, *Bioresour. Technol.,* **2012,** 122, 27.

[9] D. J. Miller, D. R. Paul, B. D. Freeman, *Polymer,* **2014,** 55, 1375.

[10] P. Kaner, E. Rubakh, D. H. Kim, A. Asatekin, *J. Membr. Sci.,* **2017,** 533, 141.

[11] D. G. Kim, H. Kang, S. Han, H. J. Kim, J.-C. Lee, *RSC Adv.,* **2013,** 3, 18071.

[12] R. Zhang, Y. Liu, M. He, Y. Su, X. Zhao, M. Elimelech, et al., *Chem. Soc. Rev.,* **2016,** 45, 5888.

[13] L.-J. Zhu, L.-P. Zhu, Y.-F. Zhao, B.-K. Zhu, Y.-Y. Xu, *J. Mater. Chem. A,* **2014,** 2.

[14] D. G. Kim, H. Kang, S. Han, J.-C. Lee, *ACS Appl. Mater. Interfaces,* **2012,** 4, 5898.

[15] D. G. Kim, H. Kang, S. Han, J.-C. Lee, *J. Mater. Chem.,* **2012,** 22, 8654.

[16] D. G. Kim, H. Kang, Y. S. Choi, S. Han, J.-C. Lee, *Polym. Chem.,* **2013,** 4, 5065.

[17] Y. S. Choi, H. Kang, D. G. Kim, S. H. Cha, J.-C. Lee, *ACS Appl. Mater. Interfaces,* **2014,** 6, 21297.

[18] H. J. Kim, D.-G. Kim, H. Yoon, Y.-S. Choi, J. Yoon, J.-C. Lee, *Adv. Mater. Interfaces,* **2015,** 2.

[19] J. J. Kim, K. Kim, Y. S. Choi, H. Kang, D. M. Kim, J.-C. Lee, *Sep. Purif. Technol.,* **2018,** 202, 9.

[20] W. J. Chen, Y. L. Su, J. M. Peng, Y. A. Dong, X. T. Zhao, Z. Y. Jiang, *Adv. Funct. Mater.,* **2011,** 21, 191.

[21] M. Lejars, A. Margaillan, C. Bressy, *Chem. Rev.,* **2012,** 112, 4347.

[22] S. Sommer, A. Ekin, D. C. Webster, S. J. Stafslien, J. Daniels, L. J. VanderWal, et al., *Biofouling,* **2010,** 26, 961.

[23] D. Hong, K. Bae, S. P. Hong, J. H. Park, I. S. Choi, W. K. Cho, *Chem Commun (Camb),* **2014,** 50, 11649.

[24] Y. Li, Y. Su, X. Zhao, X. He, R. Zhang, J. Zhao, et al., *ACS Appl. Mater. Interfaces,* **2014,** 6, 5548.

[25] P. Bengani-Lutz, I. Sadeghi, S. J. Lounder, M. J. Panzer, A.

Asatekin, *ACS Appl. Polym. Mater.,* **2019,** 1, 1954.

[26] N. K. Kim, J. Kim, D. J. Shon, J. R. Lee, Y. S. Choi, J. Yook, et al., *Eur. Polym. J.,* **2019,** 112, 688.

[27] J. Zheng, L. Li, S. Chen, S. Jiang, *Langmuir,* **2004,** 20, 8931.

[28] Q. Shao, Y. He, S. Jiang, *J. Phys. Chem. B,* **2011,** 115, 8358.

[29] A. White, S. Jiang, *J. Phys. Chem. B,* **2011,** 115, 660.

[30] J. Wu, W. Lin, Z. Wang, S. Chen, Y. Chang, *Langmuir,* **2012,** 28, 7436.

[31] A. Tuteja, W. Choi, M. Ma, J. M. Mabry, S. A. Mazzella, G. C. Rutledge, et al., *Science,* **2007,** 318, 1618.

[32] S. S. Chhatre, A. Tuteja, W. Choi, A. Revaux, D. Smith, J. M. Mabry, et al., *Langmuir,* **2009,** 25, 13625.

[33] Y. Gao, C. L. He, F. L. Qing, *Journal of Polymer Science Part a-Polymer Chemistry,* **2011,** 49, 5152.

[34] F. K. Wang, X. H. Lu, C. B. He, *J. Mater. Chem.,* **2011,** 21, 2775.

[35] C. Li, X. Li, C. Tao, L. Ren, Y. Zhao, S. Bai, et al., *ACS Appl. Mater. Interfaces,* **2017,** 9, 22959.

[36] P. H. H. Duong, K. Daumann, P. Y. Hong, M. Ulbricht, S. P. Nunes, *Langmuir,* **2019,** 35, 1284.

[37] Y. H. La, R. Sooriyakumaran, B. D. McCloskey, R. D. Allen, B. D.

Freeman, R. Al-Rasheed, *J. Membr. Sci.,* **2012,** 401, 306.

[38] M. S. Niu, R. W. Xu, P. Dai, Y. X. Wu, *Polymer,* **2013,** 54, 2658.

[39] S. M. Ramirez, Y. J. Diaz, C. M. Sahagun, M. W. Duff, O. B. Lawal, S. T. Iacono, et al., *Polym. Chem.,* **2013,** 4, 2230.

[40] D. M. Davenport, J. Lee, M. Elimelech, *Sep. Purif. Technol.,* **2017,** 189, 389.

[41] G. Hurwitz, G. R. Guillen, E. M. V. Hoek, *J. Membr. Sci.,* **2010,** 349, 349.

[42] Y. L. Jeyachandran, E. Mielczarski, B. Rai, J. A. Mielczarski, *Langmuir,* **2009,** 25, 11614.

[43] A. Asatekin, A. M. Mayes, *Environ. Sci. Technol.,* **2009,** 43, 4487.

[44] X. T. Zhao, Y. L. Su, H. Dai, Y. F. Li, R. N. Zhang, Z. Y. Jiang, *J. Mater. Chem. A,* **2015,** 3, 3325.

[45] X. T. Zhao, Y. L. Su, J. L. Cao, Y. F. Li, R. N. Zhang, Y. N. Liu, et al., *J. Mater. Chem. A,* **2015,** 3, 7287.

[46] W. Z. Ma, J. Zhang, X. L. Wang, S. M. Wang, *Appl. Surf. Sci.,* **2007,** 253, 8377.

[47] M. Elimelech, X. H. Zhu, A. E. Childress, S. K. Hong, *J. Membr. Sci.,* **1997,** 127, 101.

[48] E. M. Vrijenhoek, S. Hong, M. Elimelech, *J. Membr. Sci.,* **2001,**

188, 115.

[49] C. Hobbs, S. K. Hong, J. Taylor, *Journal of Water Supply Research and Technology-Aqua,* **2006,** 55, 559.

[50] X. Wu, Z. L. Xie, H. T. Wang, C. Zhao, D. Ng, K. S. Zhang, *RSC Adv.,* **2018,** 8, 7774.

[51] J. S. Louie, I. Pinnau, I. Ciobanu, K. P. Ishida, A. Ng, M. Reinhard, *J. Membr. Sci.,* **2006,** 280, 762.

[52] F. Fadhillah, S. M. J. Zaidi, Z. Khan, M. M. Khaled, F. Rahman, P. T. Hammond, *Desalination,* **2013,** 318, 19.

Table 2.1. Results of the synthesis of the coating polymers from different co-monomer feeding ratios.

Samples	Composition (DMAEMA:MAPOSS)[a]		M_n[b]	M_w[b]	$Đ$[b]	Solubility[c]
	In feed (mol%)	In polymer (mol%)				
PDMAEMA	100:0	100:0	15.0	29.2	1.94	S
PDM10	90:10	90:10	16.0	36.6	2.29	I
PDM15	85:15	84:16	13.5	20.7	1.54	I
PDM25	75:25	71:29	12.8	34.4	2.70	I
PDM40	60:40	65:35	12.7	35.9	2.83	I
PDM100	0:100	0:100	8.0	10.8	1.35	I

[a]Determined by ^{1}H NMR. [b]Molar mass determined by size exclusive chromatography (SEC) equipped with a refractive index (RI) detector and calibrated by using polystyrene standards (THF, 30 ºC); unit, kDa. [c]S: soluble / I: insoluble in water.

Table 2.2. XPS elemental composition (in at%) of the surfaces for the neat PSf, PDM10-, PDM15-, PSM10-, and PSM15-coated membranes.

Samples	C 1s	O 1s	N 1s	S 2p	O/C (Theo)	O/C (Exp)
PSf[a]	77.21	17.52	3.42	1.85	0.15	0.23
PDM10[b]	70.67	24.23	5.1	–[d]	0.30	0.34
PSM10[c]	66.91	25.05	3.62	4.42	0.44	0.37
PDM15[b]	74.31	22.19	3.5	–[d]	0.32	0.30
PSM15[c]	67.16	26.82	2.73	3.29	0.43	0.40

[a]neat PSf membrane. [b]After coated on the neat PSf membrane by 0.5 wt% polymer/hexane solution. [c]After post modified membrane by betainisation reaction. [d]Not detected.

Table 2.3. H_2O and CH_2I_2 contact angle values and surface energy values of the neat PSf, PDM10-, PSM10-coated membranes.

Samples	Contact angle (°)		Surface energy (γ_S)		
	H_2O	CH_2I_2	γ_S^P	γ_S^D	γ_S
PSf	72.4	18.2	4.4	48.3	52.7
PDM10	93.2	52.1	1.1	33.1	34.2
PSM10	66.4	48.5	10.7	35.1	45.8

Table 2.4. XPS elemental composition (in at%) of the surfaces of PDM10- and PSM10-coated membranes before and after long term stability test.

Samples		C 1s	O 1s	N 1s	S 2p	O/C (Exp)
Before	PDM10[a]	70.67	24.23	5.1	-[c]	0.34
	PSM10[b]	66.91	25.05	3.62	4.42	0.37
After	PDM10[a]	71.13	24.12	4.74	-[c]	0.34
	PSM10[b]	67.76	25	3.41	3.83	0.36

[a]After coated on the neat PSf membrane by 0.5 wt% polymer/hexane solution. [b]After post modified membrane by betainisation reaction. [c]Not detected.

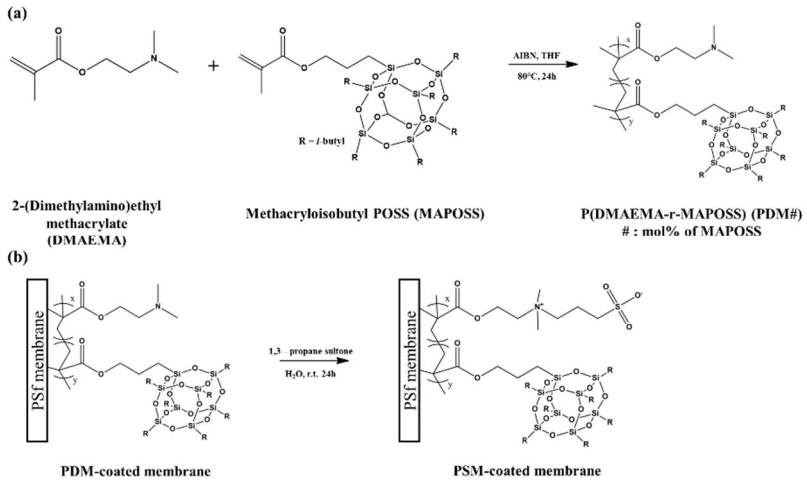

Figure 2.1. (a) Synthesis of PDM# and (b) preparation of PSM-coated membranes.

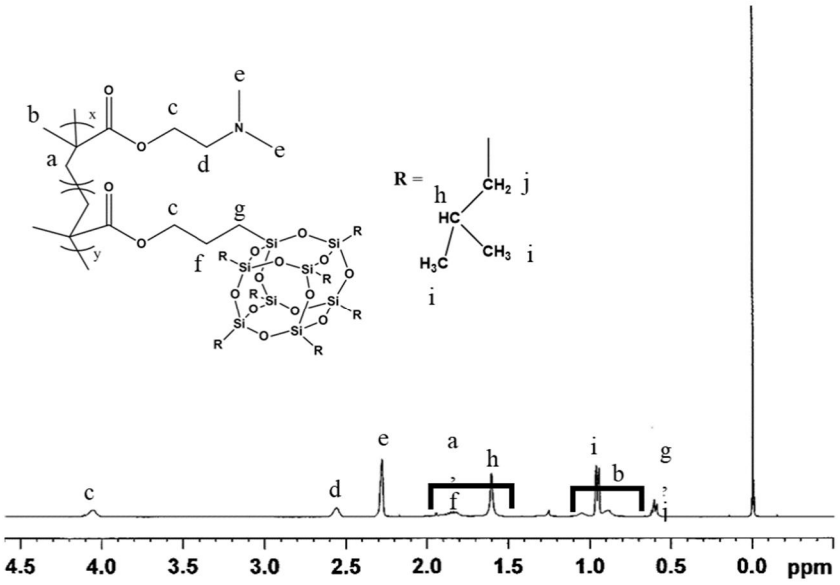

Figure 2.2. ^{1}H NMR spectrum of PDM10.

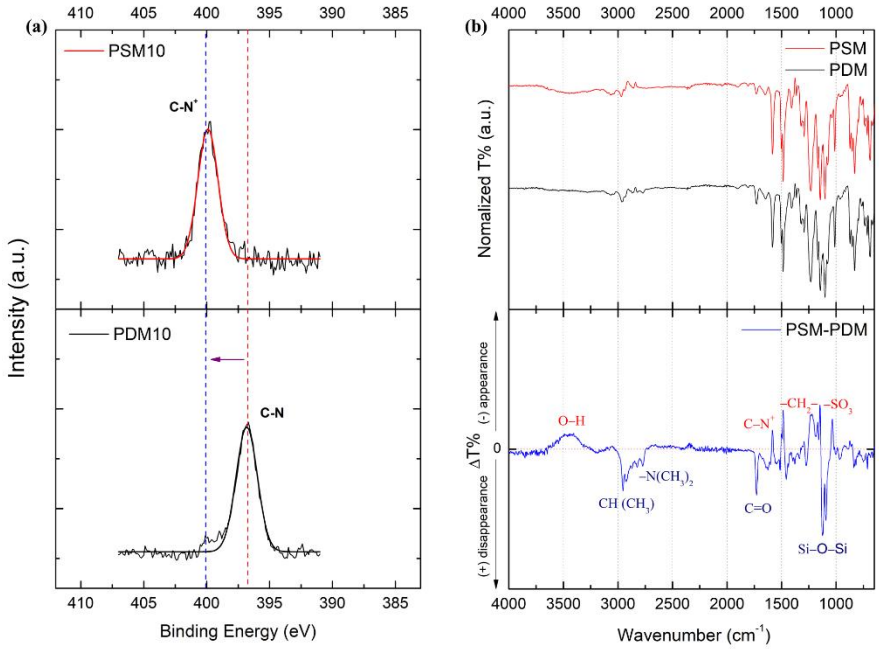

Figure 2.3. (a) The XPS results and (b) FT-IR spectrum of the PDM10- and PSM10-coated membranes (top) and difference FT-I R spectrum (PSM-PDM) (bottom).

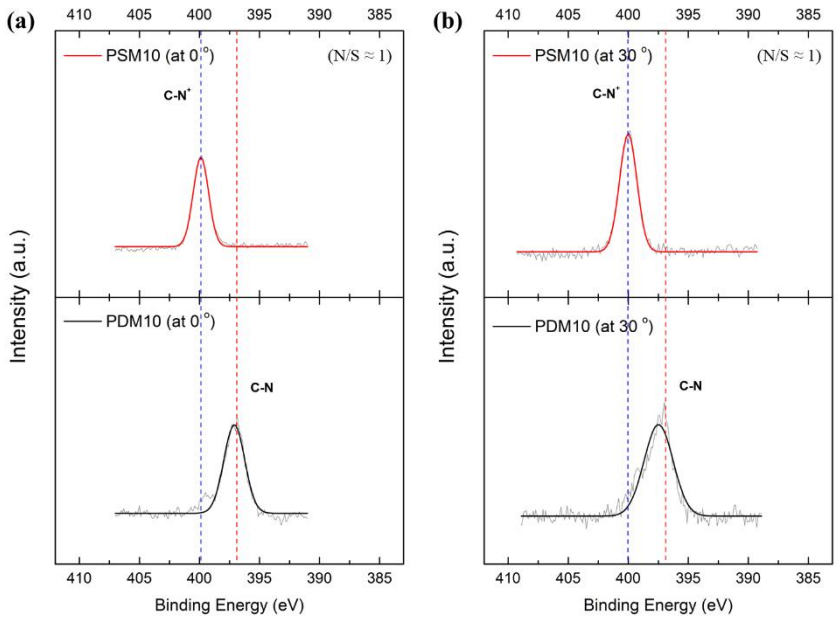

Figure 2.4. XPS results of the PDM10-, and PSM10-coated Si wafers at different angles: (a) 0° and (b) 30°.

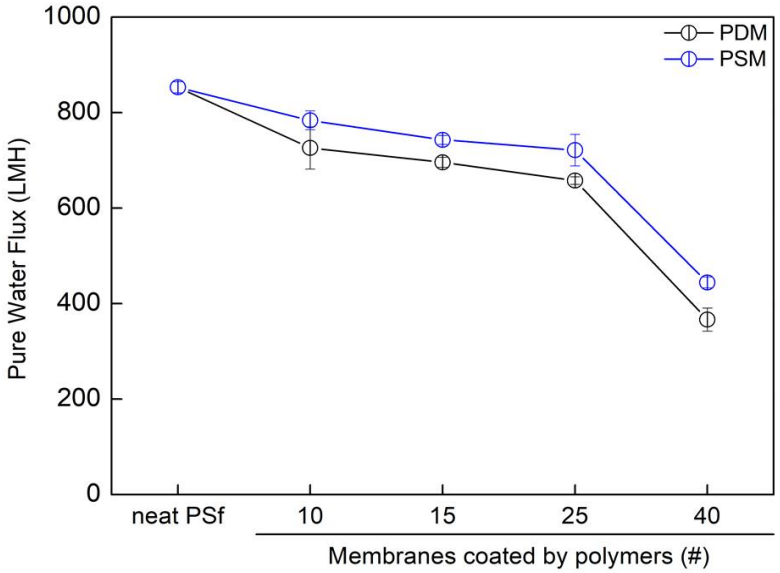

Figure 2.5. Pure water flux values of the neat PSf, PDM- and PSM-coated membranes. The filtration was performed under 1 bar at 25 ºC.

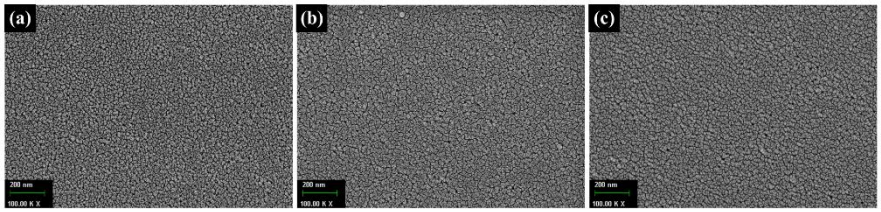

Figure 2.6. SEM images of (a) the neat PSf, (b) PDM10-, and (c) PSM10-coated membranes.

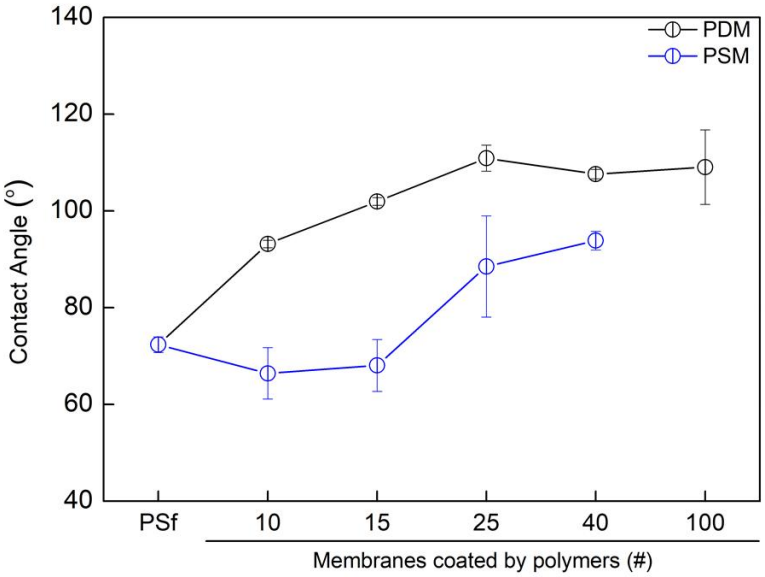

Figure 2.7. Water contact angle values of the neat PSf, PDM-, and PSM-coated membranes.

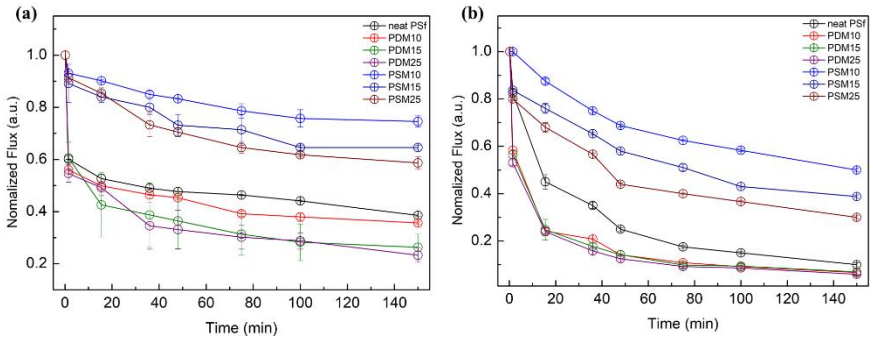

Figure 2.8. The normalized water flux of the neat PSf, PDM-, PSM-coated membranes under the filtration of (a) BSA solution (1 g L^{-1}), and (b) oil/water emulsion (0.9 g L^{-1}).

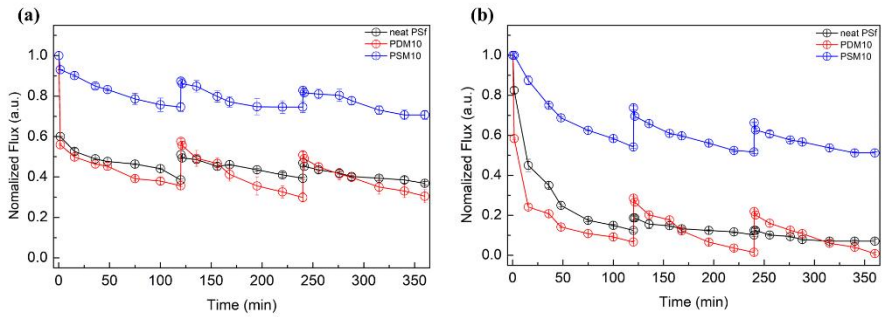

Figure 2.9. The normalized water flux behavior after cleaning with DI water at 120 and 240 min of the neat PSf, PDM10-, PSM10-coated membranes under (a) BSA solution, and (b) oil/water emulsion.

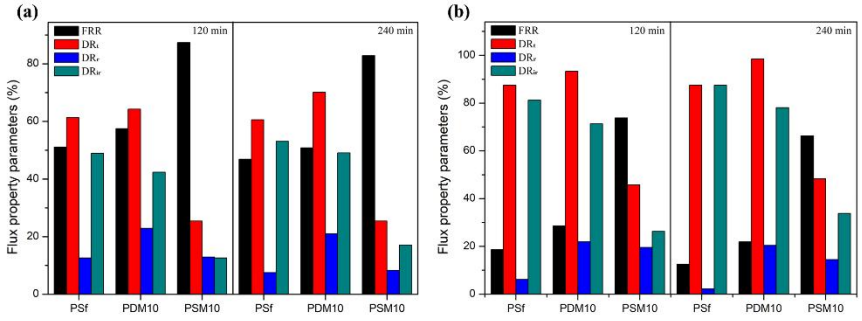

Figure 2.10. The flux property parameters for the neat PSf, PDM10-, and PSM10-coated membranes under BSA solution and oil/water emulsion.

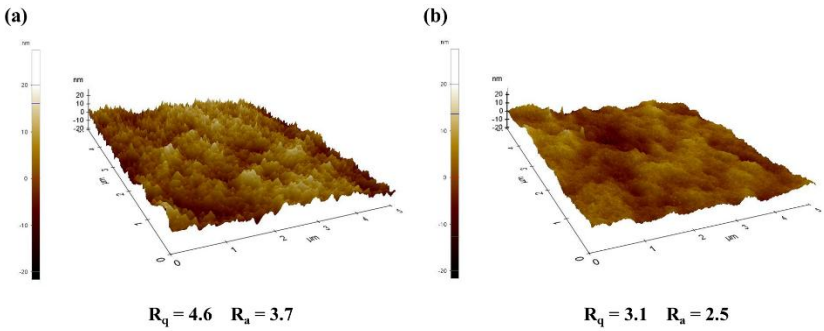

Figure 2.11. Surface topology and roughness of (a) neat PSf and (b) PSM10-coated membranes.

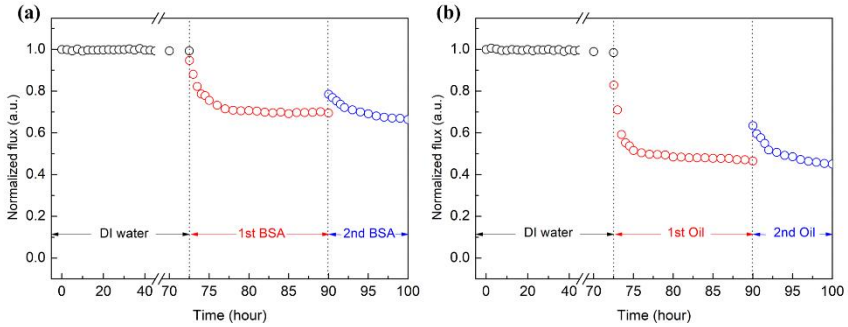

Figure 2.12. The normalized flux of PSM10-coated membrane after DI water filtration for 3 days under the filtration of (a) BSA solution (1 g L^{-1}) and (b) oil/water emulsion (0.9 g L^{-1}).

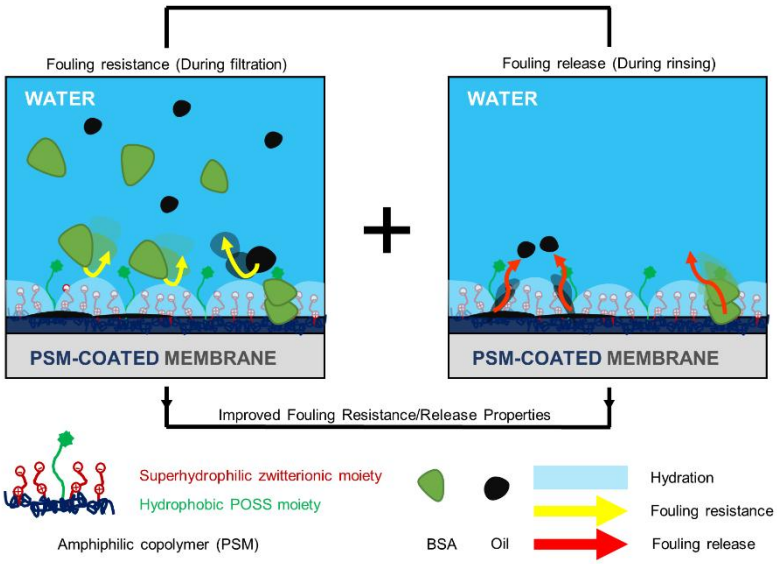

Scheme 2.1. Schematic illustration of ultrafiltration membranes coated by amphiphilic copolymers containing superhydrophilic zwitterionic and hydrophobic POSS Moieties showing improved fouling resistance/release properties.

Chapter 3

Superamphiphilic Zwitterionic Block Copolymer Surfactant-assisted Fabrication of Polyamide Thin-film Composite Membrane with Ultra-high Flux for Water Desalination

3.1. Introduction

A variety of water purification technologies including membrane filtration, thermal/membrane distillation, and electrodialysis have been developed to resolve the current global water scarcity problem.[1, 2] Among them, membrane-based technologies have received considerable attention because of the advantages such as high selectivity, low cost, low energy consumption, and fast production rate.[3, 4] Especially, the reverse osmosis (RO) membrane process using polyamide (PA) thin-film composite membranes has been widely used due to good separation efficiency, wide pH range, and excellent physical properties.[4-6]

Therefore, lots of efforts have been performed to improve membrane performances such as water flux and salt rejection by changing the interfacial polymerization (IP) parameters including monomer structure, reaction time, solvent, and additives to make more efficient PA selective layer.[7] Especially, the additives such as surfactants and fillers are effective to improve the membrane performances by altering the morphology, thickness, and/or polarity of the PA selective layer. For example, surfactants such as sodium

dodecyl sulfate (SDS) that can increase the interfacial area have been known to improve the water flux by producing more water-wettable PA selective layer.[8-15] The fillers such as carbon- and metal-based nanomaterials can also increase the water flux by changing the polarity of the PA selective layer.[16] In that regard, we had speculated that an additive working as the surfactant and filler simultaneously can improve the membrane performances synergistically, while such a multifunctional additive has not been reported to the best of our knowledge.

Block copolymers having amphiphilic properties have been widely used in the polymer nanocomposite application because they can decrease the interfacial tension between the filler and matrix as the surfactant by modifying the polarity of the filler.[17-20] However, there have been no reports on the preparation of the RO membranes using the amphiphilic block copolymers as the additive to improve the membrane performances.

In this study, we synthesized a block copolymer showing super amphiphilic characteristics containing zwitterionic and hydrophobic and used it as the additive for RO membranes. The block copolymer was found to work as the surfactant and filler simultaneously resulting

in the large increase of the water flux of the RO membrane maintaining the high salt rejection. The multifunctional role could be proved effectively by the surface analysis techniques such as contact angle (CA) measurement, optical microscope (OM), scanning electron microscope (SEM), atomic force microscopy (AFM), and X-ray photoelectron spectroscopy (XPS).

3.2. Experimental

3.2.1. Materials

2, 2-Azobisisobutyronitrile (AIBN, Junsei) was recrystallized from ethanol (EtOH, Daejung Chemicals) below 0 ºC before use. 2-(Dimethylamino)ethyl methacrylate (DMAEMA, 98%, Sigma–Aldrich) and stearyl methacrylate (SMA, TCI) were purified by passing through a syringe filter (0.2 μm, Whatman) filled with aluminum oxide (basic, for chromatography, 50 – 200 μm, Acros Organics) just before polymerization. 2-Cyano-2-propyl benzodithioate (CPDB, >97%, Sigma–Aldrich) was used as a reversible addition−fragmentation chain-transfer (RAFT) agent for the

synthesis of block copolymers. Polysulfone (PSf, Nadir® US100P from Microdyn–Nadir Corporation) ultrafiltration membrane was stored in deionized water (DI water) and used as a support membrane for the RO membranes. 1,4-dioxane (>99%, Daejung), *m*-phenylenediamine (MPD, Sigma-Aldrich), 1,3,5-benzenetricarbonyl trichloride (TMC, Sigma-Aldrich) and sodium dodecyl sulfate (SDS, > 99%, TCI), Pluronic® F108 (Sigma-Aldrich) were obtained from commercial sources and used as received. All other chemicals were used as received from Millipore–Sigma.

3.2.2. Synthesis of poly(stearyl methacrylate) (PSM) macro-RAFT agents

The following procedure was typically used for the synthesis of PSM macro-RAFT agents. For the preparation of PSM_{11} macro-RAFT agent, where 11 indicates the degree of polymerization, SMA (5.386 g, 15.9 mmol), CPDB (0.3984 g, 1.80 mmol), and AIBN (9.852×10^{-2} g, 0.6 mmol) were dissolved in 10 mL of 1,4-dioxane. This solution was added to a Schlenk flask equipped with a magnetic stirring bar and a condenser. The freeze-pump-thaw cycle was conducted 5 times for the

deoxygenation, and the mixture was then placed in an oil bath preheated at 75 °C. The mixtures were allowed to polymerize for 16 h under the nitrogen atmosphere after which it was stopped by exposure to air in an ice water bath. The resultant product was purified by precipitation in an excess cold MeOH several times. A light red product was dried under the vacuum at room temperature for several days. ^{1}H NMR [400 MHz, $CDCl_3$, δ (ppm), tetramethylsilane (TMS) ref] of PSM macro-RAFT agent: 4.13 (2H, in $–OCH_2–$), 1.56-1.95 (2H, in methacrylate backbone, in $–CH_2(CH_2)_{15}CH_3$), 1.21-1.45 (30H, in $–(CH_2)_{15}CH_3$), 0.88 - 0.90 (3H, in $CH_3C–$, $CH_3(CH_2)_{15}–$).

3.2.3. RAFT block copolymerization of poly(2-(dimethylamino)ethyl methacrylate) with PSM macro-RAFT agent.

The abbreviation of poly(stearyl methacrylate)-block-poly(2-(dimethylamino)ethyl methacrylate)) is $PSM_{\#}$-*b*-$PDM_{\#}$, where # is the degree of the polymerization (*N)*. Below is a typical procedure of the RAFT block copolymerization for the preparation of PSM_{11}-*b*-PDM_{74}. DMAEMA (4.716 g), PSM_{11} macro-RAFT agent (1.200 g), and AIBN

(0.01642 g) were dissolved in 1,4-dioxane (10 mL) and subsequently placed into a 50 mL Schlenk flask equipped with a magnetic stirring bar and a condenser. The mixture was deoxygenated by five freeze-pump-thaw cycles, and the reaction was conducted in the oil bath preheated at 75 °C for 16 h under nitrogen atmosphere. The resultant product was purified by precipitation in the excess cold hexane several times including the centrifugation. Subsequently, a solid yellow product was dried under vacuum at room temperature for several days. ^{1}H NMR [400 MHz, $CDCl_3$, δ (ppm), TMS ref] of PSM_{11}-*b*-PDM_{74}: 4.05 (2H, in $–CH_2–O$), 2.56 (2H, in $–CH_2–N(CH_3)_2$), 2.28 (6H, in $–N(CH_3)_2$), 1.56-1.95 (2H, in methacrylate backbone, in $–CH_2–(CH_2)_{15}–CH_3$), 1.21-1.45 (30H, in $–(CH_2)_{15}–CH_3$), 0.88 - 0.90 (3H, in $CH_3–C–$, $CH_3–(CH_2)_{15}–$).

3.2.4. Synthesis of water-soluble supermphiphilic zwitterionic block copolymer

For the preparation of water-soluble superamphiphilic zwitterionic block copolymer, $PSM_{\#}$-*b*-$PDM_{\#}$ was modified *via* betainisation by the treatment of 1,3-propanesultone. In brief, a solution (1.0 g/5.0 mL)

of PSM_{11}-*b*-PDM_{74} in EtOH was prepared and then the half and an equivalent of 1,3-propanesultone for the equivalent of amine units in the polymer were added while stirring in an ice bath. After 1 h, the reaction was performed in the oil bath set at 35 ºC for 24 h under the nitrogen atmosphere. The resultant product, PSM_{11}-*b*-PDM_{74}-Z50, further abbreviated PS*b*PDz (where Z50 means the average degree of zwitterionization of 50 mol% for amine units), was purified by Soxhlet extraction with EtOH and THF and dried under vacuum at room temperature for several days. ^{1}H NMR [400 MHz, D_2O, δ (ppm)]: 4.05 (2H, in $–CH_2–O$), 3.75 (2H, in $–CH_2–N(CH_3)_2–CH_2–$), 3.54 (2H, in $–CH_2–CH_2–CH_2–SO_3$), 3.08-3.29 (6H, in $–N(CH_3)_2–CH_2–$), 2.92 (2H, in $–CH_2–SO_3$), 2.67 (2H, in $–CH_2–N(CH_3)_2$), 2.25 (6H, in $–N(CH_3)_2$, and 2H, in $–CH_2–CH_2–SO_3$), 1.77-1.95 (2H, in methacrylate backbone), 0.80 - 1.12 (3H, in $CH_3–C–$).

3.2.5. Fabrication of thin-film composite membranes

The polysulfone (PSf) support membrane was immersed in the bath filled with a 2 wt% of *m*-phenylene diamine and certain amounts of PS*b*PDz dissolved aqueous solution for 5 min. Subsequently, 0.1 wt%

of trimesoyl chloride *n*-hexane solution was poured on the membrane for IP and then removed after 1 min. The membrane was moved to the 80 ºC oven for 5 min to further polymerization and thermal crosslinking reactions. The resulting membrane was washed with deionized (DI) water several times and was stored in DI water until use. Besides, to verify the effectiveness of PS*b*PDz, the neat RO membrane (without any additives), the RO membrane with SDS, and Pluronic® F108 were also prepared with the same procedure.

3.2.6. Membrane Filtration Test

Water flux and salt rejection values were measured by the lab-scale cross-flow RO membrane test unit. The effective membrane area was 4.1 × 6.1 cm^2 with a channel height of 0.3 cm. The pressure was maintained at about 15.5 bar and 2000 mg L^{-1} of NaCl solution was used as a feed solution (≈ 3.84 mS cm^{-1}). Cross-flow velocity at the membrane surface and the temperature were controlled to 1.0 L min^{-1} and 25 ºC, respectively, in the cross-flow system. Water flux (J) was calculated using **Equation 3.1**:

$$J = \Delta V/(\mathrm{A} \times \Delta t) \quad (1)$$

where ΔV is the volume of permeate collected between two weight measurements, A is the membrane surface area, and Δt is the time between two weight measurements. The salt rejection was calculated using the following **Equation 3.2**:

$$R = (1 - C_p/C_f) \times 100 \quad (2)$$

where R is the salt rejection parameter, C_p is the salt concentration in permeate, and C_f is the salt concentration in the feed. The salt concentrations were measured using a conductivity meter (HI 5321, Hanna Instruments, USA).

3.2.7. Characterization

^{1}H nuclear magnetic resonance (^{1}H NMR) spectroscopy data were obtained using Bruker Avance III 400 FT–NMR. ^{1}H NMR spectra of PSM_{11} and PSM_{11}-*b*-PDM_{74} were obtained using the $CDCl_3$ NMR solvent, while the ^{1}H NMR spectrum of PS*b*PDz was obtained using

D_2O NMR solvent. The degree of zwitterionization was calculated from the following **Equation 3.3**:

$$(Z\#) = (I_{(iii)} / 6) / [(I_{(ii)} / 6) + (I_{(iii)} / 6)] \times 100\ \% \qquad (3)$$

where $I_{(ii)}$ is the integral value of the signal (ii) assigned at 2.3 ppm corresponding to methyl protons of dimethylamine in DMAEMA units, while $I_{(iii)}$ is the integral value of the signal (iii) at 3.2 ppm corresponding to methyl protons in sulfobetaine methacrylate (SBMA) unit. Number-average and weight-average molecular weights (M_n and M_w) and the dispersity ($Đ$) were obtained by size exclusion chromatography (SEC). SEC was performed in THF (30 ºC, 1.0 mL min^{-1}) on a Waters 515 HPLC system equipped with three Polymer Laboratories columns, a PL gel 5.0 μm guard, MIXED–C, and MIXED–D in series with a Viscotek T60A refractive index detector. The resultant SEC data were analyzed using Omnisec software. To characterize micelle structure, the block copolymer was dissolved in DI water at a 0.015 wt% concentration and passed through a 0.45 μm syringe filter with the Teflon membrane before analysis. Dynamic Light Scattering (DLS) was performed on these solutions by using

DLS-7000 (Otsuka Electronics Co., Inc., Osaka, Japan) to evaluate the size distribution of 0.015 wt% PS*b*PDz in aqueous solution. The nano-scale morphologies of micelles were studied by transmission electron microscopy (TEM, JEM-3010) operated at 80.0 kV. Samples were prepared by submerging a copper grid with carbon film into the solution in DI water, followed by evaporating the solution. Contact angles from water sessile drop were measured with a Krüss DSA25 contact angle analyzer on dried membranes cut and taped onto the glass plate. The hexane in water emulsions (0.9 g of hexane in 1 L of water) were prepared by the addition of 0.015 wt% of PS*b*PDz, SDS, Pluronic® F108, and 0.1 wt% of SDS. The images were captured with a digital photomicroscope Axiophot (Zeiss Jenaval, Jena, Germany) with a 20× objective. The droplet size was analyzed using Image*J* (an open-source software). Surface morphology and topology were examined by field emission scanning electron microscope (FESEM, Carl Zeiss, SUPRA 55VP) and atomic force microscopy (AFM, Park Systems, NX–10). The surface composition of the membranes was investigated by X-ray photoelectron spectroscopy (XPS, Kratos Inc., AXIS–HSi) using Mg/Al (1486.69 eV) as the radiation source. Survey scans were conducted, followed by a high-resolution scan in the C 1s,

O 1s, N 1s, and S 2p regions, with a range of 0 – 1500 eV at an angle of 30 °.

3.3. Results and Discussion

3.3.1. Characterization of water-soluble superamphiphilic zwitterionic block copolymer surfactant

Water-soluble superamphiphilic block copolymer surfactant containing zwitterionic and long alkyl units (PS*b*PDz) was prepared through RAFT block copolymerization followed by zwitterionization using SMA to form the hydrophobic block and DMAEMA to form the hydrophilic block by the subsequent zwitterionization with 1,3-propanesultone (**Figure 3.1a**). The composition, molecular weight, dispersity, and solubility in DI water of the polymers are shown in **Table 3.1**.

When *N* of the hydrophobic SMA units is larger than 11, the resulting block copolymer is not easily soluble in water, thus it could not be used as the additive in aqueous solution for the IP process. Also, it was not possible to make the small hydrophobic block with *N* less

than 11 by the RAFT polymerization from lots of the experiments and also as reported by others.[21-24] Therefore, the optimum *N* of SMA units was decided to be 11. Since the amphiphilic block copolymer should be soluble in the aqueous phase to be used as the additive, we found that the hydrophilic block should be long enough. Meanwhile, when PSM_{11}-*b*-PDM_{74}-Z100 having the average degree of zwitterionization of 100 mol% was prepared, it was not water-soluble because of the strong intra-group, intra- and inter-chain interactions from the large length of zwitterionic units.[25-27] Therefore, *N* of the hydrophilic block was decided to be 74 with the degree of zwitterionization of 50 mol%.

Since many prior studies have reported the self-assembly behavior of amphiphilic block copolymers,[28-32] PS*b*PDz was expected to be self-assembled in aqueous solution. As shown in **Figure 3.1b**, the morphology of PS*b*PDz is a sphere with the mean number-average diameter of 45.3 nm, as indicated by the image of TEM analysis, while the z-average diameter of PS*b*PDz is about 106.5 nm with the small value of PDI (0.311). The self-assembly of PS*b*PDz in water also could be confirmed by ^{1}H NMR analysis (**Fig 3.1c**). The signal (i) assigned at 1.3 ppm corresponding to methylene protons of

SMA units is not visible in the ^{1}H NMR spectrum of PS*b*PDz dissolved in D_2O solvent because of the micelle formation consisting of the hydrophilic corona shell part covering the hydrophobic SMA core part.

3.3.2. Desalination Performance of the PA thin-film membranes fabricated with PS*b*PDz surfactant

Figure 3.2a shows membrane performances, such as water flux and salt rejection, of the RO membranes fabricated with various concentrations of PS*b*PDz in *m*-phenylenediamine aqueous solution. The flux value of the RO membrane increases from 0.68 LMH bar^{-1} to 1.69 LMH bar^{-1} by the addition of 0.015 wt% of PSbPDz. Meanwhile, when PS*b*PDz content is larger than 0.015 wt%, the flux value becomes smaller because the additional polymer acts as the impurity as observed by our previous studies on nanocomposite materials.[33-37] The flux value of the RO membrane with 0.015 wt% of PS*b*PDz is even much larger than that of the 0.1 wt% of SDS (1.0 LMH bar^{-1}), the conventional concentration and surfactant used in other studies,[38-40] indicating that PS*b*PDz is much more efficient to

increase the water flux property of the RO membrane.

The increase of the flux for the RO membranes has been explained by the increase of the surface wettability (or hydrophilicity) on PA selective layers.[9, 41, 42] Therefore, the surface wettability of the RO membranes fabricated in this study were evaluated by dynamic water CA measurement (**Figure 3.2b**).[43, 44] The degree of CA decrease is in the order of the RO membrane with PS*b*PDz > the RO membrane with SDS > the neat RO membrane, indicating that the RO membrane with PS*b*PDz is wetted better by the water than other RO membranes in this study. CA values after 140 s of water contact for the RO membranes show the same behavior (**Figure 3.2c**). The RO membranes with PSbPDz have smaller CA values than the other RO membranes, and the RO membrane with 0.015 wt% of PS*b*PDz has the smallest contact angle value and also shows the largest flux value (**Figure 3.2a**).

3.3.3. Synergistic Effects of PSbPDz surfactant working as the filler at the same time during and after IP

Since the membrane surface wettability is affected by the surface

morphology, roughness, polarity, surface composition, and other factors,[45, 46] more detailed studies on the effect of the addition of PS*b*PDz in aqueous solution for the resulting RO membranes were performed by measuring SEM, AFM, XPS, and other surface characterization techniques. We found that PS*b*PDz works as the surfactant known to improve membrane performances. At first, the surfactant in the aqueous solution can wet the surface of the hydrophobic support layers,[12] increasing the penetration of water molecules into the pores[7, 39, 47] and then producing the thinner PA selective layer without defects (**Figure 3.3a**).[8, 10-12, 15] The increase of wettability on the support layer by PS*b*PDz and SDS as the surfactants could be confirmed by measuring CA values of the DI water, PS*b*PDz aqueous solutions (0.005 – 0.03 wt%), and SDS aqueous solution (0.015 and 0.1 wt%) on the support membrane (**Figure 3.3b**), and they are about 56 º, 49 º to 47 º, and 49 º to 34 º, respectively. Therefore, PS*b*PDz and SDS can effectively work as the surfactant showing close contact angle values when PS*b*PDz and SDS have the same concentration (0.015 wt%). The increase of the water wettability by SDS and PS*b*PDz on the support layer was found to decrease the thickness of the resulting PA selective layer at the

thinnest region, as measured by cross-sectional SEM analysis (**Figure 3.4**). The thickness values of the PA selective layer at the thinnest region are in the order of the neat RO membrane (≈ 141 nm) > the RO membrane with PS*b*PDz (≈ 81 nm) > the RO membrane with SDS (≈ 73 nm).

Another explanation for the effect of the surfactant is that the surfactant located between aqueous and organic phases decreasing the interfacial tension can produce the larger ridge and valley structure of the PA selective layer because it can accelerate the transfer of amine from the aqueous to the organic phase (**Figure 3.3c**). The RO membranes with a rougher surface with larger ridge and valley structure prepared using surfactant and other techniques have been known to have larger water flux values.[9, 13, 14] As shown in the optical microscope image (**Figure 3.3d** and **3.5**), uniformly stable hexane droplets with an average diameter of about 1.91 and 1.93 μm can be seen in the mixture of hexane in water (0.9 g L^{-1}) containing 0.015 wt% of PS*b*PDz and SDS, respectively, indicating that the amphiphilic block copolymer can work as the surfactant effectively as SDS. Therefore, as measured by surface SEM and AFM analyses (**Figure 3.6a-f** and **Table 3.2**), the RO membranes with PS*b*PDz and

SDS have the rougher surfaces with larger ridge and valley structure (Rq values of 113.8 nm and 175.2, respectively), than the neat RO membrane (Rq value of 64.4). This finding may support the suggested explanations on the effects of the surfactant improving the membrane performances. Besides, since SDS was used at a higher concentration (0.1 wt%) than PS*b*PDz (0.015 wt%), the PA selective layer of the RO membrane with SDS is thinner at the thinnest region and rougher than that with PS*b*PDz. Nevertheless, the RO membrane with PS*b*PDz shows much better membrane performances with higher surface wettability than the RO membrane with SDS, indicating that PS*b*PDz might have another effect to increase the performance.

Hence, we hypothesized that PS*b*PDz would remain in the PA matrix even after the IP process due to the entanglement effect of the polymer chains with the PA matrix.[48-50] Since PS*b*PDz working as the filler could impart the additional hydrophilic pathway, the PA selective layer with PS*b*PDz should have the better water wettability, thus showing the best membrane performances. The high-resolution N 1s scans by XPS analysis were performed to investigate whether PS*b*PDz is included in the PA selective layer (**Fig. 3.7a-c**). The peak at 399.4 eV assigned to the C–N bond from the abundant amide groups of PA was

detected from all RO membranes.[51, 52] Meanwhile, the peak at 401.5 eV attributed to C–N^+ bond,[51, 52] is only seen in the result of the RO membrane with PS*b*PDz, indicating that PS*b*PDz having C–N^+ bond remains on the PA selective layer. Besides, due to PS*b*PDz including the sulfur atom, the existence of the sulfur atoms was found only in the RO membrane with PS*b*PDz (≈ 0.08 at%) (**Table 3.3**). These results clearly support the hypothesis that PS*b*PDz remains in PA selective layer after IP, increasing the wettability and consequently improving the water flux.

To the best of our knowledge, this is the first work that shows how to synthesize the water-soluble super amphiphilic block copolymer containing superhydrophilic zwitterionic and hydrophobic long alkyl moieties and investigates its effects on the membrane performances systemically as the surfactant and filler simultaneously. When a RO membrane was fabricated using 0.015 wt% of a commercially available polymer surfactant (Pluronic® F108), the flux value was found to be much smaller than that of the RO membrane with PS*b*PDz. This result could be ascribed to poorer surfactant ability[53, 54] caused by the structural characteristics having lower amphiphilicity, as observed from CA (larger angle value of 54.1°) and OM

measurements (larger average droplet diameter of and 2.23 μm) (**Figure 3.8**). Therefore, the use of PS*b*PDz having much more amphiphilicity is useful to improve membrane performance. Moreover, the results of the previous studies improving the membrane performances using various methods, such as the addition of the nanomaterials, the surface modifications, and the substrate composites, were compared with our result (**Figure 3.9**). Most of the previous studies show the trade-off behavior between water flux and salt rejection. In contrast, the RO membrane with PS*b*PDz was found to break the conventional trade-off behavior, surpassing the upper bounds of the previous studies.

3.4. Conclusions

In this study, we demonstrated that the PA thin-film composite membrane fabricated with water-soluble superamphiphilic zwitterionic block copolymer surfactant (PS*b*PDz) shows the great membrane performances. The polymer surfactant, PS*b*PDz showing the self-assembly behavior in aqueous solution due to its amphiphilicity was prepared by RAFT block copolymerization

followed by zwitterionization. The addition of PS*b*PDz in aqueous solution for the membrane fabrication *via* the IP process was found to affect the surface morphology, roughness, and polarity of the PA selective layer, resulting in the great improvement in the water flux without decreasing the salt rejection because it has the synergistic effect working as the surfactant and filler at the same time. As the surfactant, PSbPDz increases the water-wettability of the support and expands the interface region between the aqueous and organic solutions, increasing the surface roughness of the PA selective layer and making the thinnest region thinner. As the filler, PSbPDz introduced in the PA selective layer imparts additional hydrophilicity on the RO membrane producing the high-performance RO membrane with the high surface water-wettability. To the best of our knowledge, this is the first work to synthesize a novel multifunctional block copolymer surfactant working as the filler at the same time when it is used as the additive during IP for the fabrication of RO membrane and to study its effects on the RO membrane performances systemically. We believe that our results provide the expansion of amphiphilic block copolymer applications and the insight into the relationship between the additives and the performances of the RO membranes.

3.5. References

[1] M. Hightower, S. A. Pierce, *Nature,* **2008,** 452, 285.

[2] M. A. Shannon, P. W. Bohn, M. Elimelech, J. G. Georgiadis, B. J. Marinas, A. M. Mayes, *Nature,* **2008,** 452, 301.

[3] L. F. Greenlee, D. F. Lawler, B. D. Freeman, B. Marrot, P. Moulin, *Water Res.,* **2009,** 43, 2317.

[4] D. Li, H. T. Wang, *J. Mater. Chem.,* **2010,** 20, 4551.

[5] M. Elimelech, W. A. Phillip, *Science,* **2011,** 333, 712.

[6] A. J. Naaktgeboren, G. J. Snijders, J. Gons, *Desalination,* **1988,** 68, 223.

[7] W. J. Lau, A. F. Ismail, N. Misdan, M. A. Kassim, *Desalination,* **2012,** 287, 190.

[8] G. Han, S. Zhang, X. Li, N. Widjojo, T. S. Chung, *Chem. Eng. Sci.,* **2012,** 80, 219.

[9] B. Khorshidi, T. Thundat, D. Pernitsky, M. Sadrzadeh, *J. Membr. Sci.,* **2017,** 535, 248.

[10] H. I. Kim, S. S. Kim, *J. Membr. Sci.,* **2006,** 286, 193.

[11] Y. F. Li, Y. L. Su, J. Y. Li, X. T. Zhao, R. N. Zhang, X. C. Fan, et al., *J. Membr. Sci.,* **2015,** 476, 10.

[12] F. Liu, L. L. Wang, D. W. Li, Q. S. Liu, B. Y. Deng, *RSC Advances,* **2019,** 9, 35417.

[13] X. Ma, Z. Yang, Z. Yao, H. Guo, Z. Xu, C. Y. Tang, *J. Colloid Interface Sci.,* **2019,** 540, 382.

[14] W. T. Yan, M. Q. Shi, Z. Wang, Y. Zhou, L. F. Liu, S. Zhao, et al., *J. Membr. Sci.,* **2019,** 581, 168.

[15] X. Zhang, Y. Lv, H. C. Yang, Y. Du, Z. K. Xu, *ACS Appl. Mater. Interfaces,* **2016,** 8, 32512.

[16] A. K. Ghosh, B. H. Jeong, X. F. Huang, E. M. V. Hoek, *J. Membr. Sci.,* **2008,** 311, 34.

[17] J. M. Eagan, J. Xu, R. Di Girolamo, C. M. Thurber, C. W. Macosko, A. M. LaPointe, et al., *Science,* **2017,** 355, 814.

[18] M. R. Loos, J. Yang, D. L. Feke, I. Manas-Zloczower, *Compos. Sci. Technol.,* **2012,** 72, 482.

[19] M. W. Matsen, *Macromolecules,* **1995,** 28, 5765.

[20] A. Walther, K. Matussek, A. H. Muller, *ACS Nano,* **2008,** 2, 1167.

[21] M. Semsarilar, N. J. W. Penfold, E. R. Jones, S. P. Armes, *Polym. Chem.,* **2015,** 6, 1751.

[22] Y. W. Pei, O. R. Sugita, L. Thurairajah, A. B. Lowe, *RSC Advances,* **2015,** 5, 17636.

[23] V. J. Cunningham, S. P. Armes, O. M. Musa, *Polym. Chem.,* **2016,** 7, 1882.

[24] Y. Pei, L. Thurairajah, O. R. Sugita, A. B. Lowe, *Macromolecules,* **2014,** 48, 236.

[25] T. A. Wielema, J. B. F. N. Engberts, *Eur. Polym. J.,* **1987,** 23, 947.

[26] Y. Y. Jhan, R. Y. Tsay, *Journal of the Taiwan Institute of Chemical Engineers,* **2014,** 45, 3139.

[27] L. D. Blackman, P. A. Gunatillake, P. Cass, K. E. S. Locock, *Chem. Soc. Rev.,* **2019,** 48, 757.

[28] W. Zhao, G. Gody, S. M. Dong, P. B. Zetterlund, S. Perrier, *Polym. Chem.,* **2014,** 5, 6990.

[29] K. E. B. Doncom, N. J. Warren, S. P. Armes, *Polym. Chem.,* **2015,** 6, 7264.

[30] Y. Hirai, T. Terashima, M. Takenaka, M. Sawamoto, *Macromolecules,* **2016,** 49, 5084.

[31] J. Willersinn, B. Schmidt, *Polymers,* **2017,** 9.

[32] C. J. Mable, L. A. Fielding, M. J. Derry, O. O. Mykhaylyk, P. Chambon, S. P. Armes, *Chem. Sci.,* **2018,** 9, 1454.

[33] H. J. Kim, K. Choi, Y. Baek, D. G. Kim, J. Shim, J. Yoon, et al., *ACS Appl. Mater. Interfaces,* **2014,** 6, 2819.

[34] M. Y. Lim, H. J. Kim, S. J. Baek, K. Y. Kim, S. S. Lee, J.-C. Lee, *Carbon,* **2014,** 77, 366.

[35] J. Shim, D. G. Kim, H. J. Kim, J. H. Lee, J. H. Baik, J.-C. Lee, *J. Mater. Chem. A,* **2014,** 2, 13873.

[36] K. Kim, J. Bae, M. Y. Lim, P. Heo, S. W. Choi, H. H. Kwon, et al., *J. Membr. Sci.,* **2017,** 525, 125.

[37] K. H. Jung, H. J. Kim, M. H. Kim, J.-C. Lee, *Macromol. Res.,* **2020,** 28, 241.

[38] S. Hermans, R. Bernstein, A. Volodin, I. F. J. Vankelecom, *React. Funct. Polym.,* **2015,** 86, 199.

[39] S. Hermans, H. Marien, E. Dom, R. Bernstein, I. F. J. Vankelecom, *J. Membr. Sci.,* **2014,** 451, 148.

[40] V. Vatanpour, M. Safarpour, A. Khataee, H. Zarrabi, M. E. Yekavalangi, M. Kavian, *Sep. Purif. Technol.,* **2017,** 184, 135.

[41] B. Khorshidi, T. Thundat, B. A. Fleck, M. Sadrzadeh, *Sci. Rep.,* **2016,** 6, 22069.

[42] Y. Q. Wang, X. Y. Li, C. L. Cheng, Y. B. He, J. F. Pan, T. W. Xu, *J. Membr. Sci.,* **2016,** 498, 30.

[43] E. Martinelli, G. Galli, D. Cwikel, A. Marmur, *Macromol. Chem. Phys.,* **2012,** 213, 1448.

[44] S. H. Ma, J. X. Liu, Q. Ye, D. A. Wang, Y. M. Lianga, F. Zhou, *J. Mater. Chem. A,* **2014,** 2, 8804.

[45] T. Okano, M. Katayama, I. Shinohara, *J. Appl. Polym. Sci.,* **1978,** 22, 369.

[46] L. Ponsonnet, K. Reybier, N. Jaffrezic, V. Comte, C. Lagneau, M. Lissac, et al., *Mater. Sci. Eng., C,* **2003,** 23, 551.

[47] N. K. Saha, S. V. Joshi, *J. Membr. Sci.,* **2009,** 342, 60.

[48] W. W. Graessley, S. F. Edwards, *Polymer,* **1981,** 22, 1329.

[49] H. Tsukeshiba, M. Huang, Y. H. Na, T. Kurokawa, R. Kuwabara, Y. Tanaka, et al., *J. Phys. Chem. B,* **2005,** 109, 16304.

[50] P. G. Whitten, H. R. Brown, *Phys. Rev. E: Stat., Nonlinear, Soft Matter Phys.,* **2007,** 76, 026101.

[51] R. Ma, Y. L. Ji, Y. S. Guo, Y. F. Mi, Q. F. An, C. J. Gao, *Desalination,* **2017,** 416, 35.

[52] I. Abdulazeez, A. Matin, M. Khan, M. M. Khaled, M. A. Ansari, S. Akhtar, et al., *J. Membr. Sci.,* **2019,** 591.

[53] M. A. Kabong, W. W. Focke, E. L. Du Toit, H. Rolfes, S. Ramjee, *Colloids Surf., A,* **2020,** 585.

[54] S. Belbekhouche, T. Hamaide, V. Dulong, L. Picton, D. Le Cerf, J. Desbrieres, *Polym. Int.,* **2013,** 62, 1617.

[55] W. T. Yan, M. Q. Shi, Z. Wang, Y. Zhou, L. F. Liu, S. Zhao, Y. L. Ji, J. X. Wang, C. J. Gao, *J. Membr. Sci.*, **2019**, 581, 168.

[56] X. J. Song, Y. C. Wang, C. L. Jiao, M. H. Huang, G. H. Wang, H. Q. Jiang, *J. Membr. Sci.*, **2020**, 597, 117783.

[57] H. Wu, X. Zhang, X. T. Zhao, K. Li, C. Y. Yu, L. F. Liu, Y. F. Zhou, F. Zhou, C. J. Gao, *J. Membr. Sci.*, **2020**, 595, 117480.

[58] L. F. Liu, X. Xie, S. R. Qi, R. H. Li, X. Zhang, X. X. Song, C. J. Gao, *J. Membr. Sci.*, **2019**, 580, 101.

[59] T. H. Lee, J. Y. Oh, S. P. Hong, J. M. Lee, S. M. Roh, S. H. Kim, H. B. Park, *J. Membr. Sci.*, **2019**, 570, 23.

[60] H. D. Lee, H. W. Kim, Y. H. Cho, H. B. Park, *Small*, **2014**, 10, 2653.

[61] M. Ghanbari, D. Emadzadeh, W. J. Lau, T. Matsuura, A. F. Ismail, *RSC Advances*, **2015**, 5, 21268.

[62] R. Ma, Y. L. Ji, X. D. Weng, Q. F. An, C. J. Gao, *Desalination*, **2016**, 381, 100.

[63] H. M. Park, K. Y. Jee, Y. T. Lee, *J. Membr. Sci.*, **2017**, 541, 510.

[64] M. Safarpour, A. Khataee, V. Vatanpour, *J. Membr. Sci.*, **2015**, 489, 43.

[65] H. Y. Zhao, S. Qiu, L. G. Wu, L. Zhang, H. L. Chen, C. J. Gao,

J. Membr. Sci., **2014**, 450, 249.

[66] T. H. Lee, M. Y. Lee, H. D. Lee, J. S. Roh, H. W. Kim, H. B. Park, *J. Membr. Sci.*, **2017**, 539, 441.

[67] D. D. Chen, T. Y. Liu, J. Kang, R. Z. Xu, Y. Cao, M. Xiang, *Adv. Mater. Interfaces*, **2019**, 6, 1900706.

[68] J. Yin, Y. Yang, Z. Q. Hu, B. L. Deng, *J. Membr. Sci.*, **2013**, 441, 73.

Table 3.1. Polymers prepared *via* RAFT polymerization and zwitterionization.

Composition	Conv.[a]	$M_{n,SEC}$[b]	$Đ$[b]	Solubility[c]
PSM_{11}	55	4.0	1.17	I
PSM_{11}-*b*-PDM_{74}	87	15.2	1.25	I
PS*b*PDz	–	20.1[d]	–	S
PSM_{11}-*b*-PDM_{74}-Z100	–	24.6[d]	–	I

[a]Determined by ^{1}H NMR. [b]Molar mass determined by size exclusive chromatography (SEC) equipped with a refractive index (RI) detector and calibrated by using polystyrene standards (THF, 30 °C); unit, kDa. [c]S: soluble / I: insoluble in water. [d]Theoretically calculated from PSM_{11}-*b*-PDM_{74} molar mass.

Table 3.2. Surface roughness of the RO membranes with PS*b*PDz (0.000 – 0.030 wt%) and SDS (0.1 wt%).

Roughness parameter	PS*b*PDz concentration (wt%)						SDS concentration (wt%)
	0.000	0.005	0.010	0.015	0.020	0.030	0.1
R_q (nm)	64.4	95.9	112.4	113.8	102.5	82.3	175.2
R_a (nm)	51.2	73.2	87.3	88.8	81.0	63.8	138.2

Table 3.3. Surface elemental composition of the RO membranes obtained by survey scans from XPS analysis.

Samples	Element			
	C%	O%	N%	S%
Neat RO membrane	76.90 ±0.08	11.87 ±0.29	11.23 ±0.21	-[a]
RO membrane with 0.015 wt% of PSbPDz	76.74 ±0.16	12.47 ±0.17	10.71 ±0.21	0.08 ±0.04
RO membrane with 0.1 wt% of SDS	76.56 ±0.25	12.27 ±0.20	11.17 ±0.25	-[a]

[a]Not detected.

Table 3.4. Comparison of separation performances of the state-of-the-art PA TFC RO membranes.

Type	Reference	Neat		Optimum		Water flux increase rate%	Salt rejection increase rate%
		Water flux (LMH bar^{-1})	Salt rejection (%)	Water flux (LMH bar^{-1})	Salt rejection (%)		
Multifunctional Additive (PS*b*PDz)	This work	0.68	98.8	1.69	98.7	148.5	-0.1
Surfactant (SDS)	This work	0.68	98.8	1.0	98.2	47.1	-0.6
Surfactant (Pluronic® F108)	This work	0.68	98.8	0.87	98.9	27.9	0.1
Filler (Silica)	[55]	2.89	99.4	4.09	98.89	41.5	-0.5
Filler (NMPS)	[56]	2.13	98.60	3.44	98.70	61.76	0.10
Filler (Hyperbranched polymer)	[57]	2.03	98.80	3.02	98.90	49.08	0.10
Filler (UiO-66)	[58]	2.37	99.08	3.67	99.35	54.60	0.27
Filler (ZIF-9)	[59]	2.76	98.9	3.95	99.2	43.12	0.30
Filler (PDOPA coated MWCNT)	[60]	2.5	98.7	3.31	98.5	32.40	-0.20
Filler (HNTs)	[61]	1.27	97.20	2.41	95.60	90.00	-1.65
Filler (zwitterionic amine monomers)	[62]	2.0	98.9	3.6	98.3	82.3	-0.6
Support Composite (PSF/MOF)	[63]	2.33	94.00	3.03	96.00	30.32	2.13
Filler (GO)	[64]	2.29	97.40	2.97	98.16	30.03	0.78
Filler (TiO2)	[64]	2.29	97.40	3.19	93.10	39.36	-4.41
Filler (rGO/TiO2)	[64]	2.29	97.40	3.31	99.45	44.74	2.10
Filler (modified MWCNT)	[65]	0.93	95.00	1.75	90.00	88.76	-5.26
Support Composite (PSF/o-CNT)	[66]	2.24	97.40	3.03	97.70	35.27	0.31
Surface Modification (zwitterionic amino acid L-arginine)	[67]	2.84	96.42	3.97	98.10	39.73	1.74
Filler (AgNPs)	[68]	3.24	95.90	4.23	93.40	30.30	-2.61

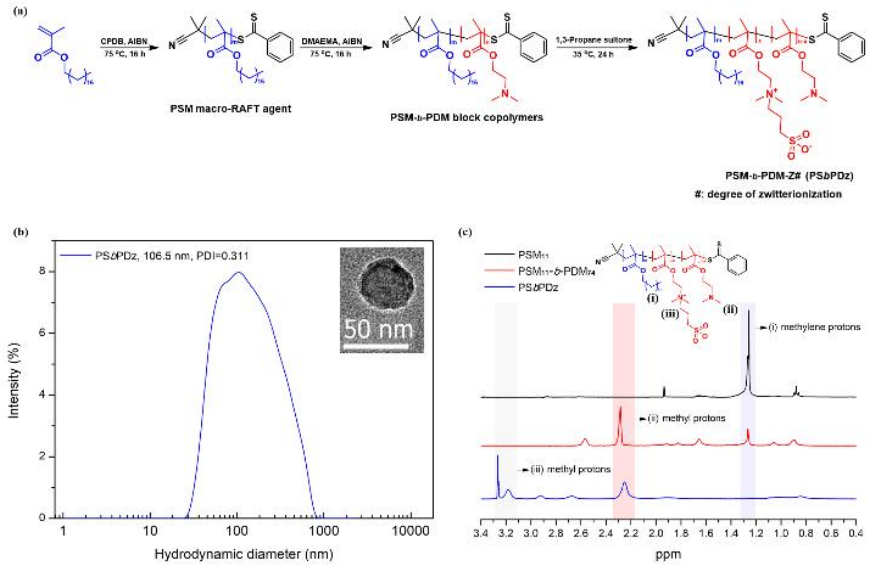

Figure 3.1. (a) Synthesis of PSM macro-RAFT agent, PSM-*b*-PDM block copolymer, and PSM-*b*-PDM-*Z*# (PS*b*PDz). (b) ^{1}H-NMR spectra of PSM_{11}, PSM_{11}-*b*-PDM_{74}, and PS*b*PDz. (c) DLS result of PS*b*PDz aqueous solution (0.015 wt%) (inset: TEM image of PS*b*PDz).

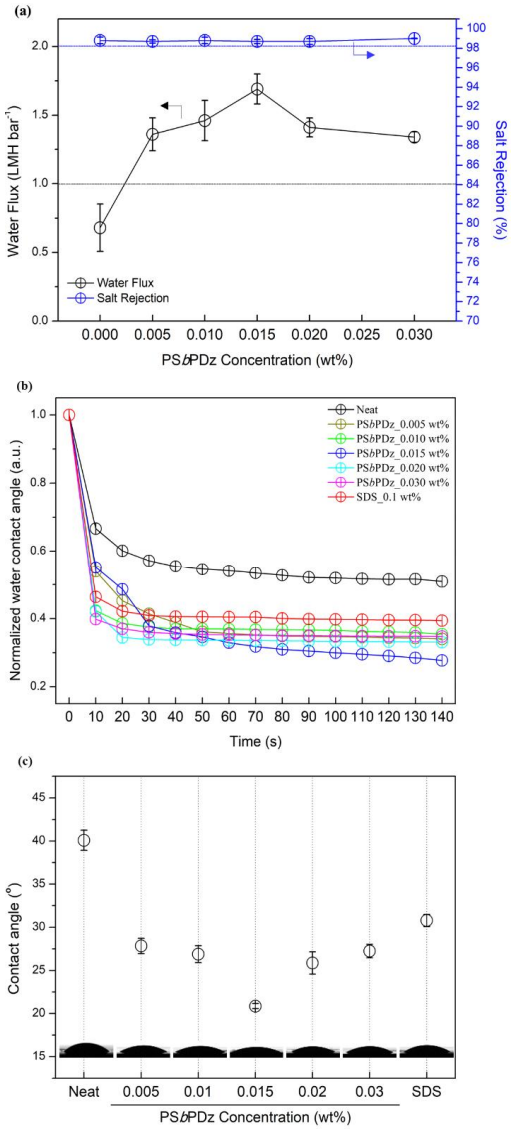

Figure 3.2. (a) Membrane performances of the RO membranes with different concentrations of PS*b*PDz (The dotted lines are the membrane performances for the RO membrane with 0.1 wt% of SDS). (b) Dynamic water contact angles of the neat RO membrane, the RO membranes with PS*b*PDz, and SDS. (c) Contact angle after 140 s for the neat RO membrane, the RO membranes with PS*b*PDz (0.015 wt%), and SDS (0.1 wt%).

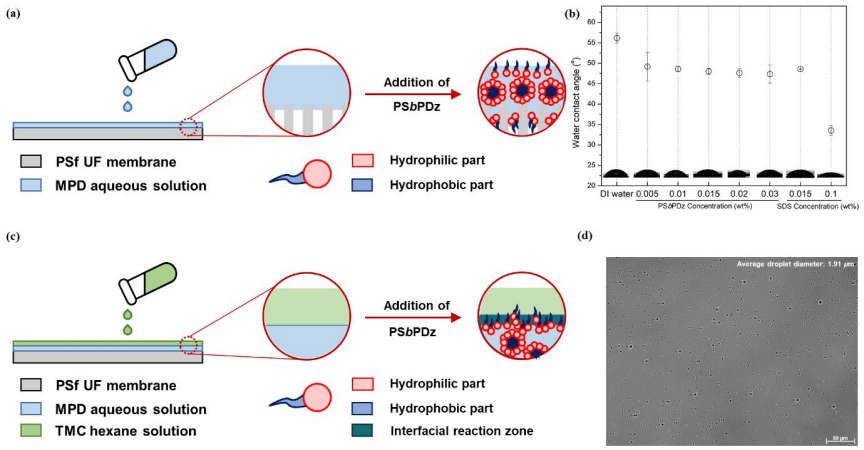

Figure 3.3 (a) Schematic diagram for the increase of the wettability of the top surface of the support membrane by the addition of PS*b*PDz. (b) Water contact angles of DI water, PS*b*PDz (0.005 – 0.030 wt%), and SDS (0.1 wt%) aqueous solutions on the support membranes. (c) Schematic diagram for the increase of the interfacial region between aqueous and organic solutions by the addition of PS*b*PDz. (d) Optical microscope image of the hexane droplets in water (0.9 g of hexane in1 L of water) containing 0.015 wt% of PS*b*PDz as the emulsifier.

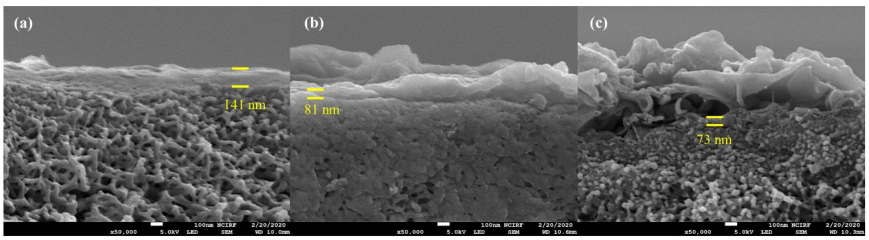

Figure 3.4. Cross-sectional SEM images of (a) the neat RO membrane, the RO membranes with (b) 0.015 wt% of PS*b*PDz, and (c) 0.1 wt% of SDS.

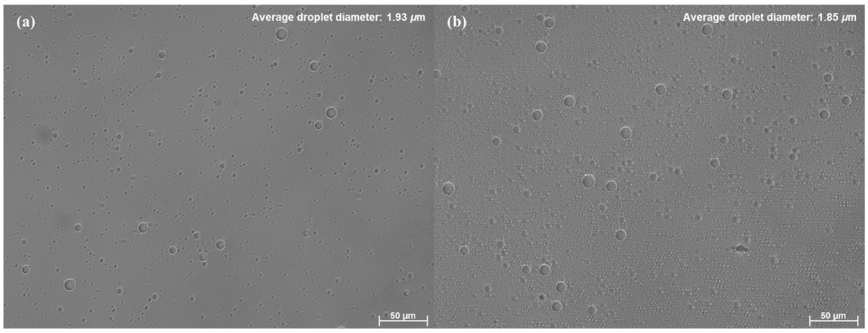

Figure 3.5. Optical microscope images of the hexane droplets in water (0.9 g of hexane in 1 L of water) containing (a) 0.015 wt% and (b) 0.1 wt% of SDS.

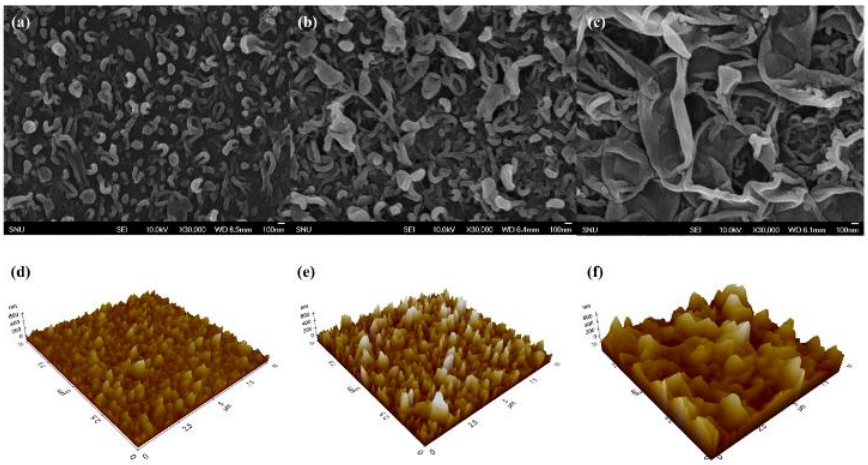

Figure 3.6 SEM images of (a) the neat RO membrane, the RO membranes with (b) 0.015 wt% of PS*b*PDz, and (c) 0.1 wt% of SDS. AFM 3D images of (d) the RO membrane, the RO membranes with (e) 0.015 wt% of PS*b*PDz, and (f) 0.1 wt% of SDS.

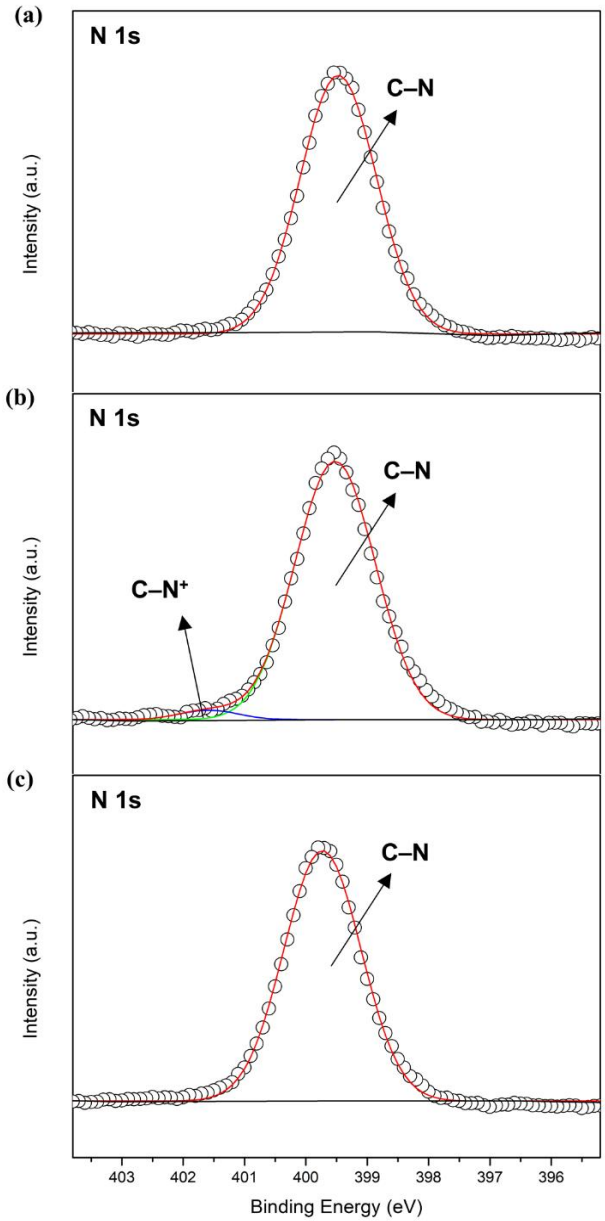

Figure 3.7. High-resolution N 1s scans of (a) the neat RO membrane, the RO membranes with (b) 0.015 wt% of PS*b*PDz, and (c) 0.1 wt% of SDS.

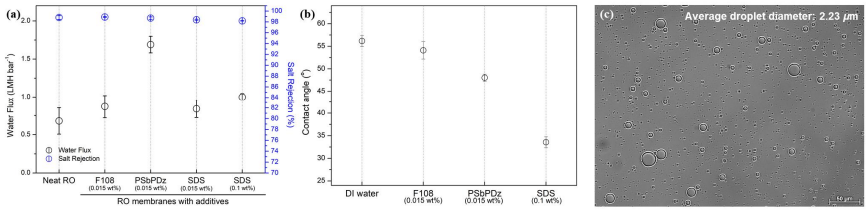

Figure 3.8. (a) Comparison of the membrane performances for the neat RO membrane, the RO membranes with 0.015 wt% of Pluronic® F108, 0.015 wt% of PS*b*PDz, 0.015 wt%, and 0.1 wt% of SDS. (b) Contact angles of DI water, 0.015 wt% of Pluronic® F108, 0.015 wt% of PS*b*PDz, and 0.1 wt% of SDS on the support membrane. (c) Optical microscope image of the hexane droplets in water (0.9 g of hexane in 1 L of water) containing 0.015 wt% of Pluronic® F108.

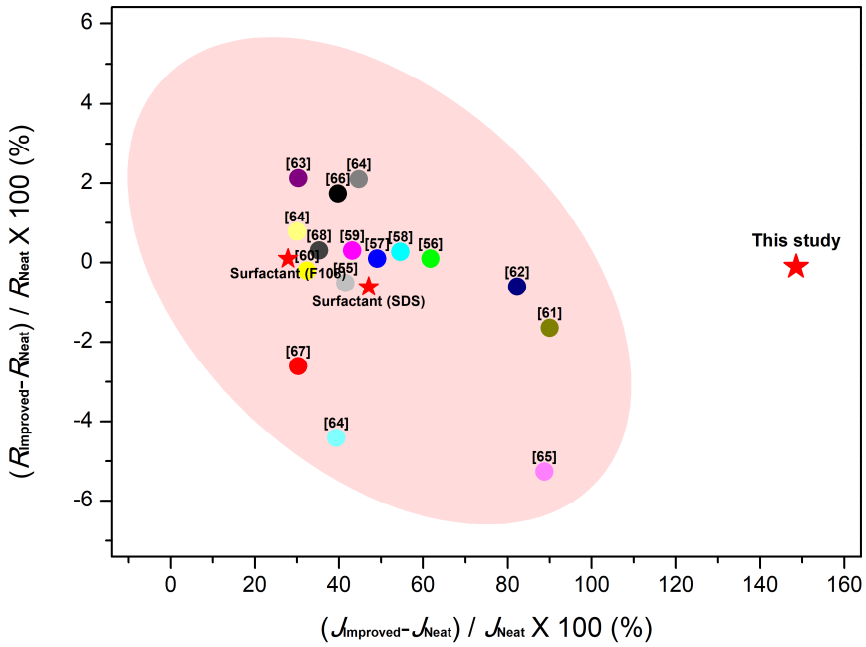

Figure 3.9. Comparison of the membrane performances of the previously reported membranes and the RO membrane with 0.015 wt% of PS*b*PDz, by the increase rates of water flux and salt rejection (for details see **Table 3.4**).

Chapter 4

Preparation of Poly(phenylene sulfide) / Nylon 6 Grafted Graphene Oxide Nanocomposites with Enhanced Mechanical and Thermal Properties

4.1. Introduction

Poly(phenylene sulfide) (PPS) has been widely used for various engineering plastics applications in batteries, automobiles, sensors, and the aerospace industry because of its superior physical and mechanical properties that originate from its structure, the aromatic rings linked by the sulfide group.[1-6] Especially, PPS composites containing glass fibers and nanomaterials have been used and studied intensively for industrial applications to overcome the brittleness.[3, 7-11]

Polymer nanocomposites prepared by mixing nano-sized filler materials with a polymer matrix have been widely studied over the last few decades because their mechanical and thermal properties could have significant advantages.[12, 13] Among nanomaterials for the polymer nanocomposite, carbon-based nanomaterials have received considerable attention in recent studies, because the carbon nanomaterials can be easily modified to increase the compatibility of the polymers with the fillers.[14-16] Graphene oxide (GO), a new class of carbon nanomaterials, has attracted tremendous interest in nanocomposite materials fields because of its unique mechanical, thermal, and electrical properties.[17-20] Furthermore, the addition of

the minimal amount of the GO derivatives in the polymer matrix can improve the performance of the nanocomposites, because of the improved specific interactions between the polymer matrix with the GO derivatives, which have a very large surface area. In addition, PPS nanocomposites reinforced by graphene-based fillers have been also studied.[5, 21, 22] Despite these advantages, increasing the compatibility of the carbon nanomaterials with the polymer matrix to obtain the polymer nanocomposites that have well-dispersed nanofillers remains a constant challenge in nanotechnology.[17, 23, 24] Notably, the dispersion of GO derivatives has been increased by various technologies including chemical modification using organic[23, 25] and polymeric moieties.[17, 26-28]

In this work, we prepared PPS nanocomposites using nylon 6 grafted graphene oxide (NGO) as a nanofiller. Nylon 6 is an aliphatic polyamide known to be mechanically blended with PPS.[29, 30] NGO was obtained by a two-step reaction including the initiation reaction between the carboxylic acid in GO with the amine group of 6-aminocaproic acid and the polymerization of ε-caprolactam (CL). The mechanical/thermal properties and the morphological characteristics of PPS/NGO nanocomposites were studied by preparing the polymer

nanocomposites with different filler contents to investigate the effect of NGO on the PPS nanocomposites.

4.2. Experimental

4.2.1. Materials

PPS pellets were kindly supplied by SK Chemical. Co., Ltd. (Korea) and used as received. GO was provided by Promico CO., Ltd. (Korea). The average particle size is 56 μm, and the degree of oxygen functionalization is 35~ 47 wt%. ε-Caprolactam (CL), 6-aminocaproic acid, and 1,1,1,3,3,3-hexafluoro-2-propanol (HFIP) were purchased from Sigma Aldrich (USA). All other reagents and solvents were used as received from standard vendors.

4.2.2. Preparation of nylon 6 grafted GO (NGO)

NGO was prepared by the procedure previously reported.[17] Briefly, NGO was obtained by the following steps: 100 mg of GO and 9.0 g of CL were added into 20.0 mL of anhydrous dimethyl formaldehyde

(DMF), and the solution was then sonicated for 1.5 h. Subsequently, 1.0 g of 6-aminocaproic acid was added to the solution under N_2 purging. Then, the flask was immersed in an oil bath controlled at 180 ºC for 1 h, and the bath temperature was raised to 250 ºC for 5 h with stirring. The products were washed with warm water several times and then purified by centrifugation with formic acid and HFIP to gain purified NGO without nylon 6 homopolymer (**Figure 4.1a**).

4.2.3. Preparation of PPS/NGO nanocomposites

PPS and NGO were melt-blended using a micro compounder operating at 90 rpm and 290 ºC for 5 min to obtain a series of PPS/NGO nanocomposites (**Figure 4.1b**). The loading amounts of NGOs in the PPS/NGO nanocomposites were 0.01, 0.03, 0.05, 0.07, and 0.09 wt%; these were named PPS/NGO001, PPS/NGO003, PPS/NGO005, PPS/NGO007, and PPS/NGO009, respectively. These nanocomposites were microinjection molded to obtain dog-bone type specimens at 60 ºC of molding temperature with 1 bar of molding pressure.

4.2.4. Characterization

Fourier transform infrared (FT-IR) spectra were recorded by a Cary 600 series FT-IR spectrometer (Agilent Technology) in the scan range of 4000-500 cm^{-1} at ambient temperature. Thermal gravimetric analysis (TGA) was performed using Q-50 from a TA instrument under N_2 atmosphere. The heating rate and temperature ranges were 10 ºC/min and 80-700 ºC, respectively. The viscosity was measured by Ubbelohde viscometer using the formic solution concentration of 3.0 g/L at 25 ºC. The dog-bone-shaped specimens of the PPS nanocomposites were prepared for the measurement of mechanical properties by using a continuous micro compounder and microinjection molding. Subsequently, the mechanical properties were measured using the universal testing machine (UTM, Instron5543, Instron instruments). The specimens were tested at room temperature under 50 % relative humidity (RH) with a test speed of 10 mm/min. Differential scanning calorimetry (DSC, Discovery DSC series, TA instruments) was used to measure the thermal behavior of the PPS/NGO nanocomposites. All DSC measurements were carried out by the following steps. The samples were heated from room

temperature to 300 ºC and cooled down to room temperature. This cycle was conducted twice to remove the thermal history of the samples. The crystallinity (X_C) of the PPS/NGO samples was calculated by the following equation:

$$X_C = \Delta H_m/[\Delta H_f(1-W_f)]\times 100\ [\%] \quad (1)$$

where ΔH_m is the melting enthalpy of completely melted nanocomposites, ΔH_f is the melting enthalpy of 100% crystalline PPS, and W_f is the mass fraction of NGO content of the nanocomposite. The fractured surface morphologies of the PPS/NGO nanocomposites were observed by a field emission scanning electron microscope (FESEM, Carl Zeiss, SIGMA) with an energy dispersive spectrometer (EDS) analysis. The magnification of all SEM images is 5000× and the scale bars are 2 μm.

4.3. Results and Discussion

4.3.1. Preparation of NGO

As shown in **Figure 4.1a**, nylon 6 chains were grafted onto GO by the *in situ* ring-opening polymerizations of CL using 6-aminocaproic acid as an initiator. In the initiation step, the amine groups of 6-aminocaproic acid react with both the carboxylic groups and the epoxy groups in GO. Since the nylon 6 homopolymer could be formed by the homopolymerization of CL, purification steps such as centrifugation and washing using HFIP, which can dissolve only the nylon 6 homopolymer, were conducted.[31] The color change from brown of GO to the black of NGO was observed after the reaction, as shown in **Figure 4.2**. GO looks brown because many of the conjugated π bonds of graphene are oxidized,[18] whereas NGO looks black because those oxidized units are reduced by the reaction at 180 to 250 ºC that is known to be high enough to reduce the oxygen functional groups of GO.[17] FT-IR curves further confirmed the reaction from GO to NGO, as shown in **Figure 4.3a**. GO shows a strong and broad absorption peak at around 3400 cm^{-1} from the hydroxyl groups including carboxylic acid and water molecules in GO, as well as a C=O peak at 1720 cm^{-1}. NGO shows additional peaks from C=O (1630 cm^{-1}), C-N (1530 cm^{-1}), and C-H (2930 and 2860 cm^{-1}) stretching vibrations. The char residue value of NGO was found

to be larger than that of GO from TGA as shown in **Figure 4.3b**. Since many of the oxygen functional groups in GO are reduced and/or decomposed during the polymerization at high temperature (250 ^{o}C),[32] NGO having much less oxygen functional groups than GO have larger char yield value.[17] The peak intensities from the oxygen functional groups such as hydroxyl groups from carboxylic acid and alcohol (3400 and 1370 cm^{-1}, respectively) and epoxy groups (1224 cm^{-1}) in FT-IR spectra of NGO are much smaller than those of GO.

The grafting length of nylon 6 in NGO could be estimated by measuring the viscosity of nylon 6 homopolymer extracted during the washing steps by formic acid and HFIP as reported in the previous study,[17] using the inherent viscosity (η_{inh}) and Mark-Houwink equation as the following equation:[31]

$$\eta_{inh} = KM_{\eta}^{\alpha} \quad (2)$$

where M_{η} is the viscosity-average molecular weight, and K and α (the Mark-Houwink parameters) are 2.26×10^{-4} and 0.82, respectively.[33] As shown in **Table 4.1**, the calculated M_{η} of nylon 6 is about 8,640 g/mol indicating that the number of repeating units in the polymer is

about 77. The relative content of nylon 6 in NGO was measured by TGA analysis. For NGO, the weight loss below 250 ºC is different from that of GO, because most of the oxygen-containing functional groups in GO are reduced and/or modified during the ring-opening polymerization at the high temperature of 250 ºC. Therefore, the weight loss below 450 ºC about 22 % can be attributed to the decomposition of the grafted nylon 6 chains in NGO, which is corresponding to the relative content of nylon 6 in NGO.[34] Using two properties such as the grafting length and relative content of nylon 6 in NGO, the grafting density (δ), the number of the polymer chains per area of nanofiller surface, can be also calculated using the following equation:

$$\text{Grafting density } (\delta) = [M/A] \times [M_p/M_{nf}] \times [N_A/M_w] \times 10^{-18} \quad [\text{chains/nm}^2] \qquad (3)$$

where M/A is the mass per unit area of a graphene sheet (7.7×10^{-4} g/m^2), M_p/M_{nf} is the relative mass fraction of grafted polymers in nanofillers measured from TGA analysis, N_A is the Avogadro constant, and M_w is the molecular weight of the grafted polymer. Therefore, the

grafting density of nylon 6 in NGO is 0.015 chains/nm^2, and this value is close to those obtained by others by their studies of the nanofillers having polymer chains.[35, 36]

4.3.2. Thermal and mechanical properties of PPS/NGO nanocomposites

The thermal properties of PPS/NGO nanocomposites measured by DSC and TGA are listed in **Table 4.2**. The melting temperature (T_m), the crystallization temperature (T_c), and the decomposition temperature for 5 wt% loss ($T_{d,5\%}$) and 30 wt% loss ($T_{d,30\%}$) values indicate that NGO in the PPS matrix can increase the thermal transition temperatures as observed by others in their polymer nanocomposite studies using carbon nanomaterials.[7, 21, 28] However, we could not observe any obvious trend of the changes of the transition temperature or the initial decomposition temperature ($T_{d,5\%}$) according to the change of the content of NGO as observed by others form their nanocomposite studies,[37] although the largest T_m value of 281 ºC was observed from the PPS/NGO nanocomposite having 0.03 wt% of NGO in the PPS matrix (PPS/NGO003).

Meanwhile, the decomposition temperature for 30 wt% loss ($T_{d,30\%}$) shows the obvious trend that $T_{d,30\%}$ increases with the increase of the contents of NGO in PPS. Similar results were also observed by Liang et al. in their nanocomposite studies.[38] Interestingly, the largest tensile strength and elongation at break values were also observed from PPS/NGO003, as shown in **Figures 4.4** and **4.5**. Possibly, 0.03 wt% of NGO in PPS/NGO nanocomposite is the optimum content to give the toughest structure leading to the highest T_m. A similar correlation between T_m and mechanical strength was observed by others in their studies of graphene-based polymer nanocomposites.[4, 31, 39, 40] However, PPS/NGO003 does not show the largest T_c, X_C, and $T_{d,5\%}$ values, whereas such a mismatch between the mechanical properties and crystallization characteristics or decomposition for the polymer nanocomposites has also been observed by others for various reasons.[4, 17, 21, 38, 40, 41] Although the optimum contents of NGO for the thermal transition and decomposition temperature are different, NGO was found to increase the thermal stability of PPS. It is well known that graphene-based or GO-based fillers in the polymer matrix can increase the thermal stability because the phenol moieties in graphene can capture the radicals generated during the thermal

decomposition and the sheet-like structure can retard the thermal degradation of the polymer. It should be also noted that the char residue at 600 ºC (ω) of the PPS and PPS nanocomposites were found to be irrelevant to their initial decomposition temperature, and the char residue values of the nanocomposites were always smaller than that of neat PPS, as shown in **Figure 4.6**. Since PPS itself has an excellent char-forming capability,[42] the addition of the NGO to the PPS can disrupt the char-formation ability of PPS upon heating. A similar phenomenon was reported by others and is explained by the retardance of the fillers on the aromatization for the generation of compact char.[17, 41, 43, 44]

The mechanical properties of PPS and PPS/NGO nanocomposites measured by UTM are shown in **Table 4.2**, **Figures 4.4,** and **4.5**. The tensile strength and the elongation at break values of PPS/NGO nanocomposites increase as the content of NGO increases, and the maximum values of 56.8 MPa and 8.9 %, respectively, were observed when the NGO content was 0.03 wt%. Further increase of NGO content decreased these values, and when the NGO content was larger than 0.07 wt%, these values were even smaller than those of PPS without any filler. Obviously, when the PPS/NGO nanocomposite had

the optimum content of the fillers, 0.03 wt% of NGO, the fillers were well-dispersed in the polymer matrix by the increased interactions between the nylon 6 chains in NGO and the PPS chains in the matrix.[17, 26] However, when the NGO content was larger than 0.07 wt%, the tensile strength and the elongation at break values of the PPS/NGO nanocomposites became smaller than those of PPS, because when the contents of nanofillers are larger than a certain value, they are aggregated in the polymer matrix, forming segregated domains that decrease these mechanical properties.[20, 45]

Interestingly, the PPS/NGO nanocomposite with an optimum content of NGO (0.03 wt%) that gave the largest melting temperature and mechanical toughness showed the smallest Young's modulus value (890 MPa) among the samples. In general, nanofillers including GO derivatives in the polymer matrix increase the tensile strength and Young's modulus values, whereas they decrease the elongation at break values when the polymer nanocomposites have the optimum amount of the fillers. Our unusual result can be explained by the physical strength of nylon 6 grafted on NGO and the mechanically blending of nylon 6 with the PPS matrix.[46] Since the mechanical strength of nylon 6 is smaller than that of PPS, the introduction of the

nylon 6 moiety into the PPS matrix can decrease Young's modulus value of PPS. In contrast, since nylon 6 chains in NGO can be entangled with PPS chains, the increased interaction between NGO and PPS can increase the toughness, such as the tensile strength and the elongation at break values. According to our previous study, when 0.01 wt% of nylon 6 grafted GO was added into the polyketone, which has higher mechanical strength, the resulting polyketone nanocomposite showed improved toughness, whereas its Young's modulus value was found to be smaller than that of pristine polyketone for the same reason.[17]

The percolation threshold, the critical filler volume fraction when the first percolating path forms through the polymer matrix,[47, 48] of the PPS/NGO nanocomposites could be estimated by Young's modulus curve (**Figure 4.7**) plotted as the function of NGO volume fraction. The density values of NGO and PPS (1950 kg/m^3 and 1350 kg/m^3, respectively) could be used to obtain the volume fraction from the weight fraction. In the percolation approach, the mechanical properties have been known to be closely related to a percolation-like scaling law around the percolation threshold: [48]

$$E = E_0 + A(\phi - \phi_c)^t \quad (4)$$

where E is Young's modulus, ϕ is the NGO volume fraction, ϕ_c is the percolation threshold, and A and t are constants. As can be seen from the fitting curve (red line) in Figure 4, the percolation threshold is ϕ_c = 0.021 vol% (0.031 wt%) while the percolation exponent is t = 1.4. The other mechanical properties such as tensile strength and elongation at break can be affected by the formation of such the network. Interestingly, the values of these properties increase with the increment of the NGO volume fraction until the percolation threshold and then decrease drastically with the further increase of NGO. This result could be attributed to the reduced mobility of the polymer chains in the vicinity of the NGO surface resulting in premature failure.[48]

4.3.3. Morphology of PPS/NGO nanocomposites

The morphology of the fractured surface of PPS/NGO nanocomposites can further explain the mechanical behavior of the nanocomposites, as shown in **Figure 4.8**. The fractured surface of the neat PPS is relatively flat and smooth because the typical brittle

fracture morphology of the polymers weakly resist crack initiation and propagation (**Figure 4.8a**).[18] However, the fractured surfaces become rougher with the addition of NGO, indicating that the PPS/NGO nanocomposite is less brittle than neat PPS. Also, any agglomeration of NGO is not observed (**Figures 4.8b**, and **4.8c**), indicating that NGO is well-dispersed in the PPS matrix for the PPS/NGO001 and PPS/NGO003, resulting in the increased toughness. Meanwhile, further addition of NGO generates the aggregates, because of the typical agglomeration characteristic of nanomaterials,[20] as shown in **Figures 4.8d-f**. The aggregates of nanofillers in the polymer matrix act as defects to decrease the toughness of the polymer matrix. EDS mapping analysis was performed to analyze the aggregates further, as shown in Figure 6. PPS consists of carbon, hydrogen, and sulfur, whereas NGO is composed of carbon, hydrogen, oxygen, and nitrogen. Therefore, sulfur and nitrogen can be the key elements for observing the aggregation of NGO. As shown in **Figure 4.9a**, the EDS mapping image of neat PPS shows the uniform dispersion of the sulfur atoms in all regions, and no nitrogen signal is seen. Also, the sulfur and nitrogen atoms are uniformly shown in all-region in the EDS mapping

image of PPS/NGO003 (**Figure 4.9b**). However, those of PPS/NGO009 (**Figure 4.9c**) shows that the signals of sulfur and nitrogen atoms are located in different regions, because of the aggregates of NGO in the PPS matrix. Therefore, the agglomeration of NGO in the matrix decreases the toughness of the polymer matrix.[20]

4.3.4. The toughening mechanism for PPS/NGO nanocomposites

Furthermore, the toughening mechanism for polymer nanocomposites can be generally explained by the existence of the sacrificial bonds such as hydrogen bonds, ionic bonds, Van der Waals interaction, and hydrophobic interaction. These additional bonds can be sacrificially dissociated when the load applied in polymer nanocomposites, resulting in releasing the hidden length at the interface between nanofillers and polymer matrix.[49] Interestingly the divalent sulfur atom is known to act as the hydrogen bond acceptor,[50, 51] then sulfide in PPS can form the hydrogen atom in amide groups in nylon 6. The FT-IR analysis was used to examine the additional sacrificial bonds between NGO and PPS in PPS/NGO

nanocomposite, as shown in **Figure 4.10**. The small shift of at 1074 cm^{-1} corresponding to the C-S bonds in PPS[52] was observed in the PPS/NGO nanocomposites due to the hydrogen bonding between sulfur atoms in PPS and hydrogen atoms in amides of NGO. The existence of the hydrogen bonding in PPS/NGO nanocomposites can increase the toughness up to when 0.03 wt% of the NGO is added, but the toughness decreases when larger than 0.03 wt% of NGO was added because of the aggregation of NGO.

4.3.5. Comparison of NGO and GO for the filler materials

PPS/GO nanocomposite with the GO content of 0.03 wt%, the same amount of NGO in the PPS/NGO nanocomposites that showed maximum toughness, was prepared, and the mechanical property and thermal stability of the PPS/GO nanocomposite were compared with those of PPS/NGO nanocomposite to investigate the effect of NGO, as shown in **Figure 4.11**. Although both GO and NGO increased the mechanical toughness and thermal stability of PPS, PPS/NGO003 showed more tensile strength and elongation at break values than did PPS/GO003, indicating that NGO is a better filler to increase the

mechanical toughness and the thermal stability. Since the nylon 6 chains in NGO can be entangled with PPS chains and help NGO to be dispersed in the PPS matrix better than GO does, the well-dispersed NGO acts as the barrier against deformation or decomposition when tensile stress or high thermal energy is applied.

4.4. Conclusions

PPS/NGO nanocomposites were prepared for the first time to investigate the effect of NGO on the mechanical and thermal properties of the polymer nanocomposites, where NGO was prepared by ring-opening polymerization using ε-caprolactam in the presence of GO. Since the nylon 6 chains in NGO can be entangled with PPS chains, the addition of only 0.03 wt% of NGO into the PPS matrix increases toughness, such as the 32 % and 30 % increase of the tensile strength and elongation at break values, respectively. Similarly, 0.03 wt% NGO in PPS was found to be the optimum content to give the highest melting temperature of the PPS/NGO nanocomposites. These results were attributed to the well-dispersed NGO in the PPS matrix, as was confirmed by observation of the fractured surface of PPS/NGO

nanocomposites through SEM and EDS mapping analysis. Comparing the mechanical toughness and thermal stability of PPS/NGO and PPS/GO nanocomposites, NGO was found to be a more effective filler. Finally, we believe that PPS/NGO nanocomposites are promising as engineering plastics because of their increased toughness and thermal stability.

4.5. References

[1] W. Luo, Q. Liu, Y. Li, S. T. Zhou, H. W. Zou, M. Liang, *Compos. Part B: Eng.,* **2016,** 91, 579.

[2] M. Rule, D. R. Fagerburg, J. J. Watkins, P. B. Lawrence, *Markromol. Chem., Rapid Commun.,* **1991,** 12, 221.

[3] H. Wang, J. Zhao, Y. Zhu, Y. Meng, Y. Zhu, *J. Colloid Interface Sci.,* **2013,** 402, 253.

[4] B. Caglar, P. Fischer, P. Kauranen, M. Karttunen, P. Eisner, *J. Power Sources,* **2014,** 256, 88.

[5] S. L. Deng, Z. D. Lin, B. F. Xu, W. P. Qiu, K. Y. Liang, W. Li, *J. Therm. Anal. Calorim.,* **2014,** 118, 197.

[6] S. Z. D. Cheng, Z. Q. Wu, B. Wunderlich, *Macromolecules,* **1987,** 20, 2802.

[7] J. W. Gu, Y. Q. Guo, X. T. Yang, C. B. Liang, W. C. Geng, L. Tang, et al., *Compos. Part A: Appl. Sci. Manuf.,* **2017,** 95, 267.

[8] J. Xing, Q. Q. Ni, B. Y. Deng, Q. S. Liu, *Compos. Sci. Technol.,* **2016,** 134, 184.

[9] H. Zou, N. Ning, R. Su, Q. Zhang, Q. Fu, *J. Appl. Polym. Sci.,* **2007,** 106, 2238.

[10] J. Choi, S. Lim, J. Kim, C. R. Choe, *Polymer,* **1997,** 38, 4401.

[11] Z. Chen, T. Li, Y. Yang, X. Liu, R. Lv, *Wear,* **2004,** 257, 696.

[12] J. Q. Pham, C. A. Mitchell, J. L. Bahr, J. M. Tour, R. Krishanamoorti, P. F. Green, *J. Polym. Sci. Part B: Polym. Phys.,* **2003,** 41, 3339.

[13] M. Huskic, M. Zigon, *Eur. Polym. J.,* **2007,** 43, 4891.

[14] F. H. Gojny, M. H. G. Wichmann, U. Köpke, B. Fiedler, K. Schulte, *Compos. Sci. Technol.,* **2004,** 64, 2363.

[15] C. Wu, X. Y. Huang, G. L. Wang, X. F. Wu, K. Yang, S. T. Li, et al., *J. Mater. Chem.,* **2012,** 22, 7010.

[16] K. S. Novoselov, A. K. Geim, S. V. Morozov, D. Jiang, Y. Zhang, S. V. Dubonos, et al., *Science,* **2004,** 306, 666.

[17] M. Y. Lim, H. J. Kim, S. J. Baek, K. Y. Kim, S. S. Lee, J. C. Lee, *Carbon,* **2014,** 77, 366.

[18] S. Stankovich, D. A. Dikin, R. D. Piner, K. A. Kohlhaas, A. Kleinhammes, Y. Jia, et al., *Carbon,* **2007,** 45, 1558.

[19] K. Kim, J. Bae, M. Y. Lim, P. Heo, S. W. Choi, H. H. Kwon, et al., *J. Membr. Sci.,* **2017,** 525, 125.

[20] J. R. Potts, D. R. Dreyer, C. W. Bielawski, R. S. Ruoff, *Polymer,* **2011,** 52, 5.

[21] J. Xing, B. Deng, Q. Liu, *High Perform. Polym.,* **2017,** 30, 519.

[22] C.-Y. Chang, S.-P. Ju, J.-W. Chang, S.-C. Huang, H.-W. Yang, *RSC Advances,* **2014,** 4, 26074.

[23] H. J. Kim, K. Choi, Y. Baek, D. G. Kim, J. Shim, J. Yoon, et al., *ACS Appl. Mater. Interfaces,* **2014,** 6, 2819.

[24] S. Park, J. An, I. Jung, R. D. Piner, S. J. An, X. Li, et al., *Nano Lett.,* **2009,** 9, 1593.

[25] Y. F. Xu, Z. B. Liu, X. L. Zhang, Y. Wang, J. G. Tian, Y. Huang, et al., *Adv. Mater. (Weinheim, Ger.),* **2009,** 21, 1275.

[26] T. Ko, K. Kim, M. Y. Lim, S. Y. Nam, T. H. Kim, S. K. Kim, et al., *J. Mater. Chem. A,* **2015,** 3, 20595.

[27] M. Y. Lim, H. Shin, D. M. Shin, S. S. Lee, J. C. Lee, *Polymer,* **2016,** 84, 89.

[28] W. H. Liao, S. Y. Yang, J. Y. Wang, H. W. Tien, S. T. Hsiao, Y. S. Wang, et al., *ACS Appl. Mater. Interfaces,* **2013,** 5, 869.

[29] K. C. Mai, S. C. Zhang, Q. F. Gao, H. M. Zeng, *J. Appl. Polym. Sci.,* **2000,** 78, 1579.

[30] S. F. Zhou, Q. X. Zhang, C. Q. Wu, J. Huang, *Mater. Des.,* **2013,** 44, 493.

[31] Z. Xu, C. Gao, *Macromolecules,* **2010,** 43, 6716.

[32] W. Gao, L. B. Alemany, L. Ci, P. M. Ajayan, *Nat. Chem.,* **2009,** 1, 403.

[33] G. B. Gechele, A. Mattiussi, *Eur. Polym. J.,* **1965,** 1, 47.

[34] S. V. Levchik, G. Camino, L. Costa, G. F. Levchik, *Fire Mater.,* **1995,** 19, 1.

[35] L. Y. Kan, Z. Xu, C. Gao, *Macromolecules,* **2011,** 44, 444.

[36] R. C. Chadwick, U. Khan, J. N. Coleman, A. Adronov, *Small,* **2013,** 9, 552.

[37] V. H. Pham, T. T. Dang, S. H. Hur, E. J. Kim, J. S. Chung, *ACS Appl. Mater. Interfaces,* **2012,** 4, 2630.

[38] Q. Liu, W. Luo, Y. Chen, H. Zou, M. Liang, *High Perform. Polym.,* **2016,** 29, 889.

[39] J. Bian, Z. J. Wang, H. L. Lin, X. Zhou, W. Q. Xiao, X. W. Zhao, *Compos. Part A: Appl. Sci. Manuf.,* **2017,** 97, 120.

[40] M. El Achaby, F.-E. Arrakhiz, S. Vaudreuil, A. el Kacem Qaiss, M. Bousmina, O. Fassi-Fehri, *Polym. Compos.,* **2012,** 33, 733.

[41] M. Y. Lim, J. Oh, H. J. Kim, K. Y. Kim, S. S. Lee, J. C. Lee, *Eur. Polym. J.,* **2015,** 69, 156.

[42] L. H. Perng, *Polym. Degrad. Stab.,* **2000,** 69, 323.

[43] J. Alam, M. Alam, M. Raja, Z. Abduljaleel, L. A. Dass, *Int. J. Mol. Sci.,* **2014,** 15, 19924.

[44] K. Yang, X. Huang, L. Fang, J. He, P. Jiang, *Nanoscale,* **2014,** 6, 14740.

[45] J. A. Nairn. Matrix Microcracking in Composites. In: Talreja R, Manson J-A, editors. Polymer Matrix Composites: Elsevier Science; 2000.

[46] S. Akhtar, J. L. White, *Polym. Eng. Sci.,* **1992,** 32, 690.

[47] A. Noël, J. Faucheu, J.-M. Chenal, J.-P. Viricelle, E. Bourgeat-Lami, *Polymer,* **2014,** 55, 5140.

[48] K. Nawaz, U. Khan, N. Ul-Haq, P. May, A. O'Neill, J. N. Coleman, *Carbon,* **2012,** 50, 4489.

[49] R. Q. Liu, S. M. Liang, X. Z. Tang, D. Yan, X. F. Li, Z. Z. Yu, *J. Mater. Chem.,* **2012,** 22, 14160.

[50] T. Schaefer, S. R. Salman, T. A. Wildman, P. D. Clark, *Can. J. Chem.,* **1982,** 60, 342.

[51] D. L. Howard, H. G. Kjaergaard, *Phys. Chem. Chem. Phys.,* **2008,** 10, 4113.

[52] D. A. Zimmerman, J. L. Koenig, H. Ishida, *Spectrochim. Acta, Part A,* **1995,** 51, 2397.

Table 4.1. NGO properties.

Nylon 6 in NGO		Relative content of nylon 6 in NGO (%)	Grafting density (chains/nm2)
Inherent viscosity (η_{inh})	Molecular weight (M_η)		
0.381	8,640	22	0.015

Table 4.2. Thermal and mechanical properties of neat PPS and PPS/NGO nanocomposites

Sample	Tc (oC)	Tm (oC)	X_c (%)	Td,5% (oC)	Td,30% (oC)	ω (%)	Tensile strength (MPa)	Young's modulus (MPa)	Elongation at break (%)
PPS	218.9	278.4	56.3	481.3	523.6	48.1	43.1 ± 8.1	1180 ± 190	6.9 ± 2.5
PPS/NGO001	224.9	279.6	61.7	490.5	535.4	45.1	47.2 ± 11.6	1080 ± 180	7.3 ± 2.6
PPS/NGO003	225.7	281.2	57.9	488.3	535.9	45.4	56.8 ± 10.3	890 ± 70	8.9 ± 2.3
PPS/NGO005	225.1	279.7	59.8	489.5	536.7	45.4	52.4 ± 11.4	970 ± 130	7.5 ± 2.1
PPS/NGO007	225.9	279.2	57.9	484.9	538.4	46.2	29.0 ± 8.0	1240 ± 90	4.2 ± 1.3
PPS/NGO009	224.4	279.7	60.6	487.1	536.8	46.1	29.8 ± 2.4	1230 ± 60	4.1 ± 0.4

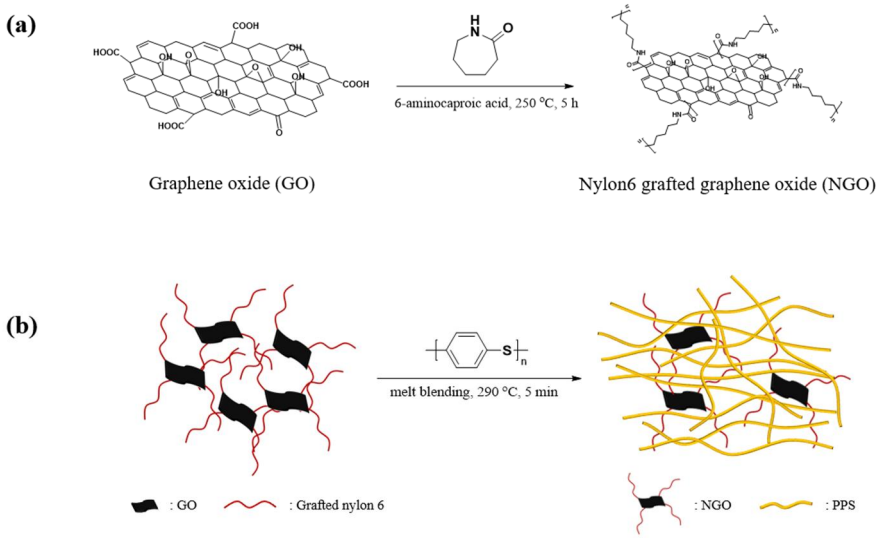

Figure 4.1. Synthetic routes to (a) nylon 6 grafted graphene oxide (NGO) and (b) poly (phenylene sulfide) / nylon 6 grafted oxide (PPS/NGO) nanocomposite.

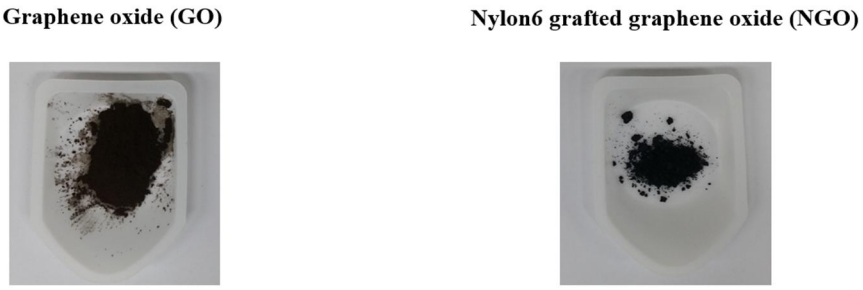

Figure 4.2. Digital images of GO and NGO.

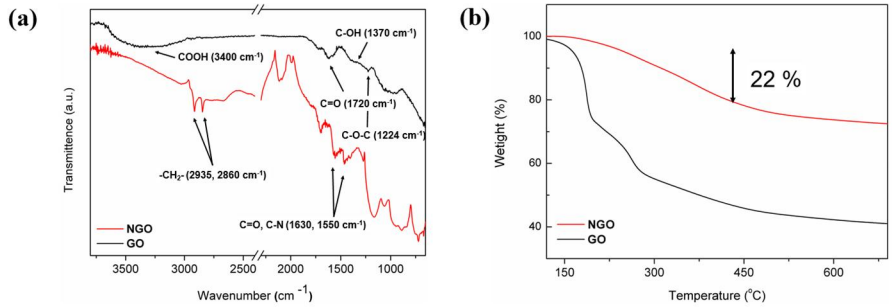

Figure 4.3. Characterization of GO and NGO: (a) FT-IR spectra and (b) TGA curves.

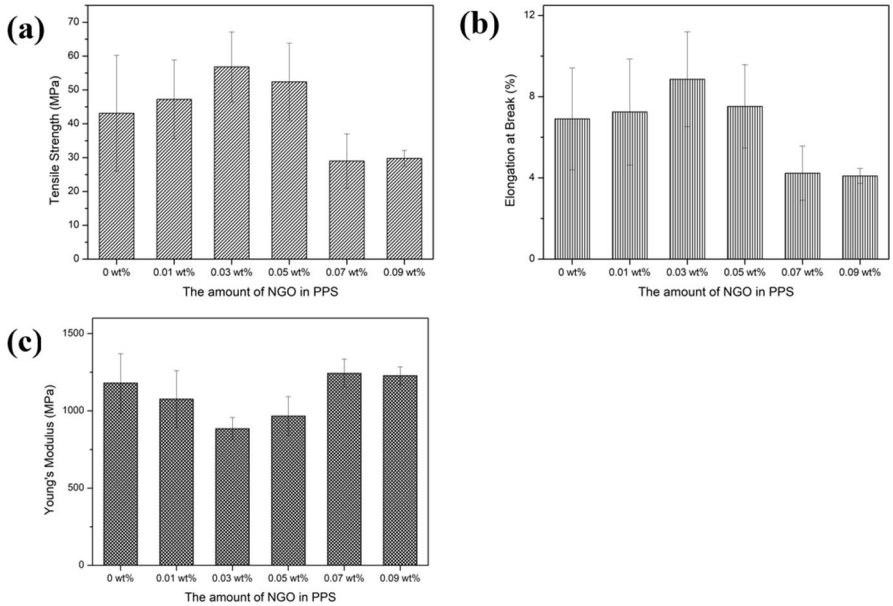

Figure 4.4. Mechanical properties of PPS and PPS/NGO nanocomposites: (a) tensile strength, (b) elongation at break, and (c) Young's modulus.

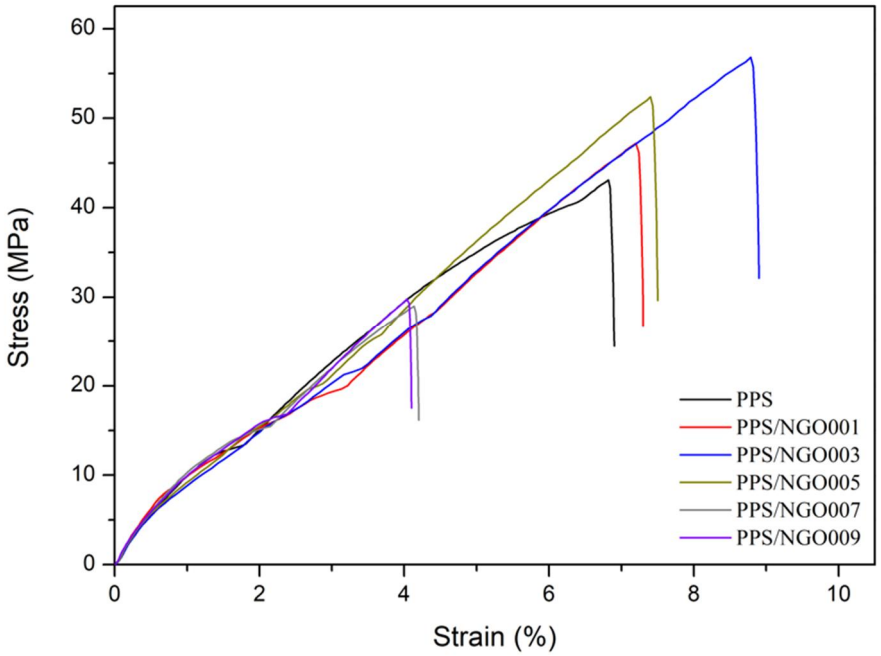

Figure 4.5. Stress-strain curves of PPS and PPS/NGO nanocomposites.

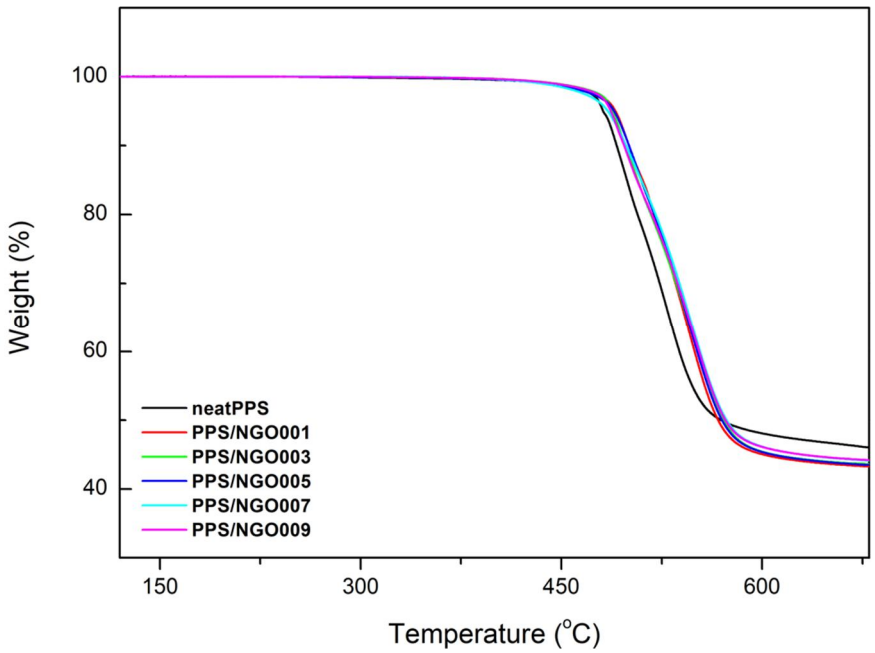

Figure 4.6. TGA curves of neat PPS and PPS/NGO nanocomposites.

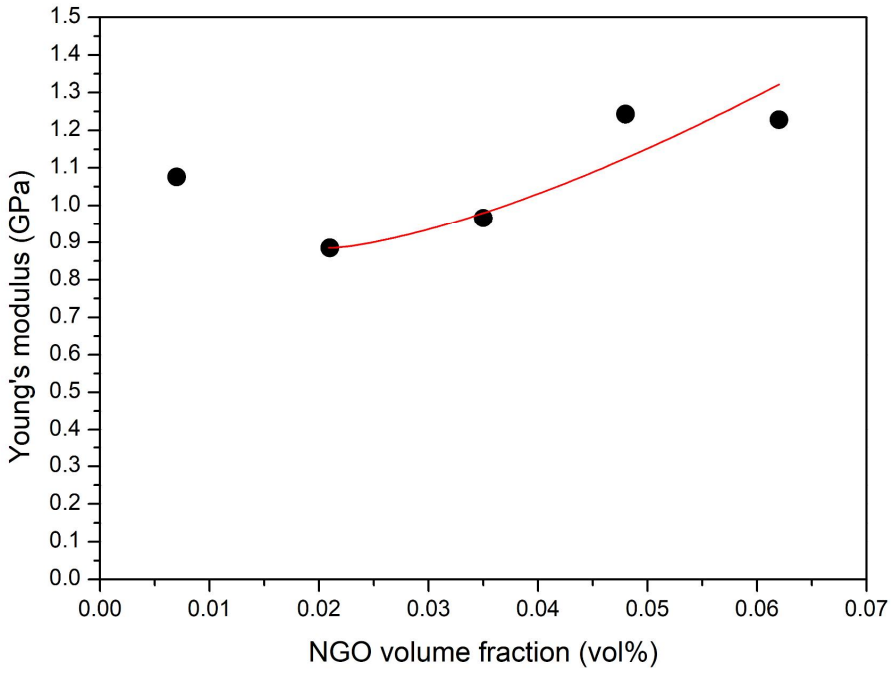

Figure 4.7. Young's modulus plotted as a function of NGO volume fraction. The red line illustrates the percolation behavior of the PPS/NGO nanocomposites.

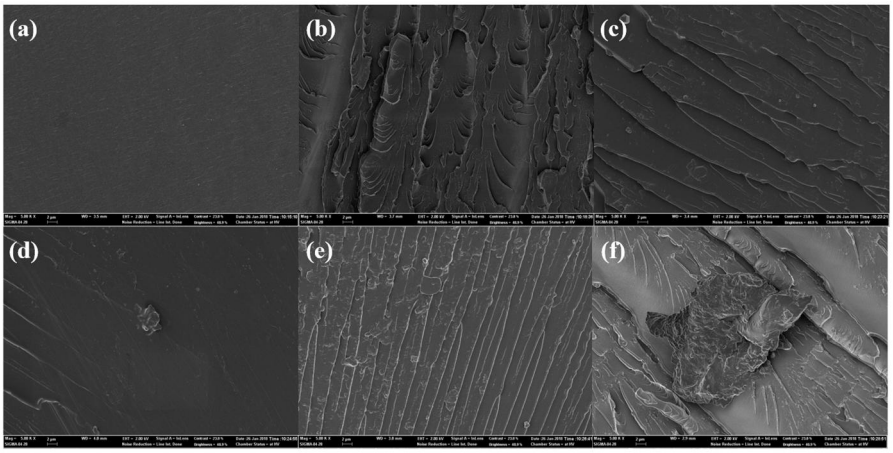

Figure 4.8. SEM images of fractured surfaces: (a) neat PPS, (b) PPS/NGO001, (c) PPS/NGO003, (d) PPS/NGO005, (e) PPS/NGO007, and (f) PPS/NGO009

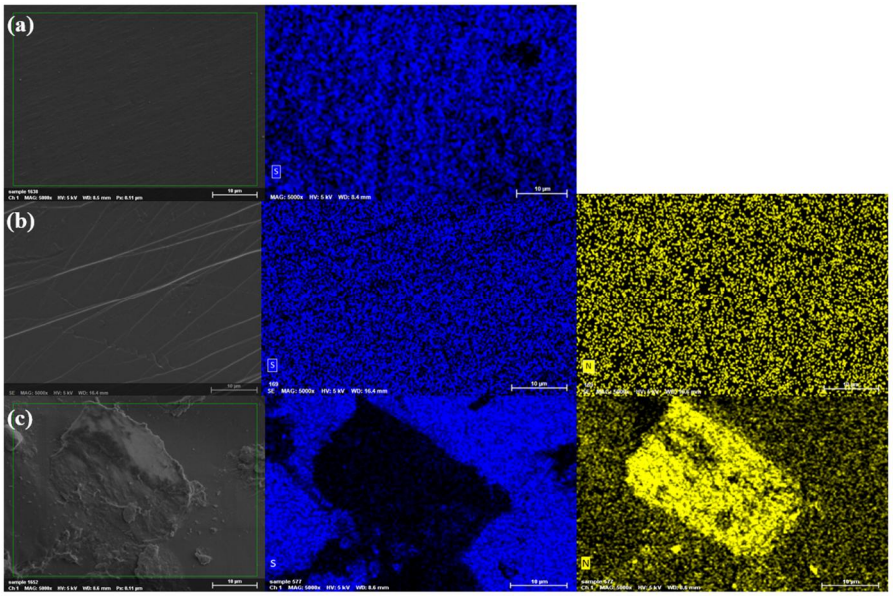

Figure 4.9. EDS mapping images of (a) neat PPS, (b) PPS/NGO003, and (c) PPS/NGO009

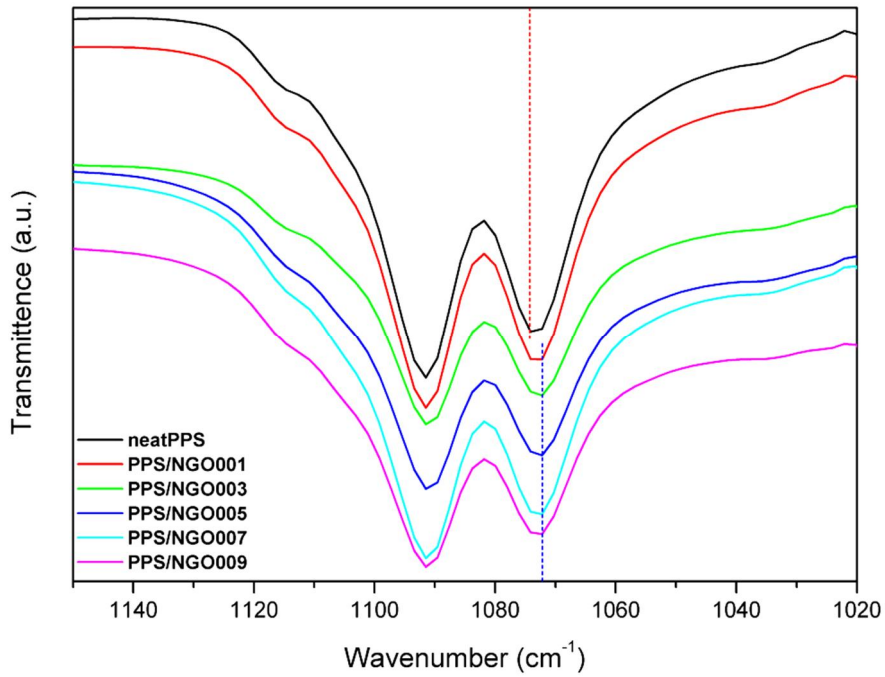

Figure 4.10. FT-IR spectra for neat PPS and PPS/NGO nanocomposites.

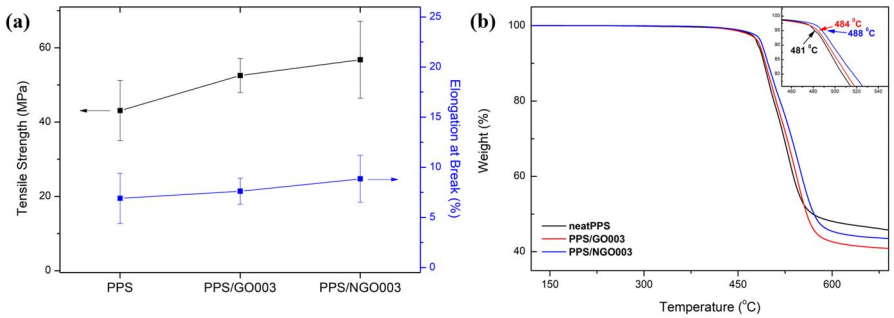

Figure 4.11. Comparison of PPS and PPS nanocomposites in (a) mechanical properties and (b) thermal stability.

초 록

본 논문은 계면 활성을 지닌 양친매성 고분자계 재료들의 합성과 분석, 그리고 한외여과막과 역삼투막과 같은 수처리 막 및 고분자 나노복합체로의 응용에 대하여 기술하였다. 첫째, 초친수성 양쪽성 이온기 부분과 소수성 POSS 부분을 함유하는 양친매성 공중합체가 코팅된 한외여과막 (PSM 코팅막) 을 제조하였다. 2-(디메틸아미노)에틸 메타크릴레이트 (DMAEMA) 와 POSS 메타크릴레이트 (MAPOSS) 의 서로 다른 조성들을 함유하는 일련의 공중합체(PDM)를 준비하기 위하여 자유 라디칼 공중합 방법을 이용하였다. PDM이 코팅된 막에 존재하는 DMAEMA 단위체들은 이후에 1,3-프로페인 술톤을 이용하여 추후-양쪽성이온화 반응을 통해 술포베타인 메타크릴레이트 (SBMA) 단위체로 개질되었으며 결과적으로 PSM이 코팅된 막을 제조할 수 있었다. 이렇게 제조된 PSM이 코팅된 막은 가장 좋은 오염 저항/방출 물성을 보였다. 향상된 오염 저항성은 양쪽성이온들과 물 분자간의 강한 전기적인 상호작용을 통해 막 표면에 수화층을 형성할 수 있는 초친수성 양쪽성 이온기 부분에 의한 것임을 밝혔다. 또한, PSM이 코팅된 막의 전체 표면 에너지 (γ_S) 값 역시

아무것도 코팅되지 않은 폴리술폰막보다 작았는데 이는 소수성의 POSS기 부분 때문이었으며, 이로 인해 가장 뛰어난 오염 방출 특성을 보였다.

두 번째, 폴리아미드 박막 역삼투막 제조에 사용하는 전형적인 계면활성제를 대체하고자 초친수성 양쪽성이온기와 소수성 긴 알킬기 단위체들을 포함하는 수용성 초양친매성 블록 공중합체 계면활성제 (PS*b*PDz) 를 가역적 첨가−단편화 사슬 이동 공중합법을 이용하여 합성하였다. PS*b*PDz는 계면활성제로써 성공적으로 활용되는 것을 확인하였고, 폴리아미드 매트릭스와 고분자 사슬의 얽힘 효과를 통해 계면 중합 이후에서 필러로써 동시에 사용되는 것 확인하였다. 계면활성제로써는, PS*b*PDz는 지지체 표면의 습윤성을 향상시키고 수용액과 유기 용액 사이의 계면을 확장시켜 제조된 폴리아미드 선택층의 두께를 감소시키고 표면 거칠기를 증가시키는 효과를 불러왔다. 필러로써는, 폴리아미드 선택층에 도입된 PS*b*PDz는 역삼투막 표면의 습윤성을 향상하는 역할을 했음을 확인하였다. 따라서, 계면 중합을 통해 수용액에 PS*b*PDz를 일정량 용해시켜 제조된 역삼투막은 가장 큰 수투과도 값을 보였고 높은 염제거율 값을 유지하는 성능을 보였다.

마지막으로, 개시 작용기로 작용하는 카르복실 산 작용기를 가지는 그래핀 옥사이드 (GO) 표면에 ε-카프로락탐의 고리개환 중합을 통해서 제조된 나일론 6가 그래프팅된 GO (NGO)와 폴리페닐렌 설파이드의 나노복합체를 마이크로컴파운딩을 통해 제조하였다. 나일론 6는 PPS와 혼합하여 상용화된 것으로 알려져 있기 때문에, NGO의 나일론 6 부분은 PPS의 기계적 물성을 향상시킬 수 있고, 특히 PPS/NGO 나노복합체의 향상된 인성을 초래하였다. 더 나아가, 그래핀 나노시트는 향상된 기계적 강도와 열적 안정성을 제공할 수 있는데 그 이유는 그래핀 나노시트의 기계적 강화효과와 열적 장벽 역할 때문이다. 그 결과, PPS/NGO 나노복합체는 인장 강도와 파단신율과 같은 기계적 강도가 가장 좋은 것으로 확인되었고 열적 안정성 역시 강화되었다. 이러한 향상된 물성들은 PPS 매트릭스 내에서 잘 분산된 NGO에 의한 것이며, 이는 SEM과 EDS 맵핑 분석을 활용한 형상학 분석을 통해서 확인되었다.

주요어: 표면 코팅, 양친매성 양쪽성 랜덤 공중합체, 수 처리, 막,

방오성, 박막 복합체, 양친매성 양쪽성 블록 공중합체, 계면활성제, 필러, 담수화, 폴리페닐렌 설파이드, 그래핀 옥사이드, 엔지니어링 플라스틱, 나노복합체

학 번: 2014-22620